

**Role of Phospholipase D in Idiopathic Pulmonary Fibrosis and FTIR Imaging to Detect
Fibrogenesis**

BY

VIDYANI SURYADEVARA

B.Tech., Osmania University, India, 2013

M.S., University of Illinois at Chicago, USA 2014

THESIS

Submitted as partial fulfillment of the requirements
for the degree of Doctor of Philosophy in Bioengineering
in the Graduate College of the
University of Illinois at Chicago, 2018

Chicago, Illinois

Defense Committee:

Dr. Viswanathan Natarajan, Chair and Advisor, Department of Pharmacology & Medicine

Dr. Thomas J Royston, Department of Bioengineering

Dr. Dieter Klatt, Department of Bioengineering

Dr. Micheal J Walsh, Department of Pathology

Dr. Andrea Balla, Department of Pathology

I dedicate this thesis to all aspiring, independent young women

ACKNOWLEDGEMENT

This incredible journey helped me grow as a person.

Firstly, I thank my parents and brother for their continual support throughout my PhD. The strength and emotional support imbibed by them is incredible.

I'm blessed to have worked with Drs. Viswanathan Natarajan and Thomas Royston as my advisors during my PhD. This journey in the pursuit of my PhD with them has made me evolve as a person and a researcher. Dr. Natarajan has given me a wonderful PhD experience by allowing me to be engaged in multiple research projects not only in his laboratory, but with other investigators as well, which enabled broadening of my scientific pursuits. Dr. Royston made me more self-confident and unleashed my strengths. Thank you for introducing me to the world of Bioengineering.

Dr. Walsh has given me an opportunity to integrate with his laboratory to work on the FT-IR project, an integral part of my thesis which was a big learning curve for me. I thank Shaiju S Nazeer for his tremendous help with the analysis. David, Hari Sreedhar have also been instrumental when I got started in the lab.

I thank Dr. Andrea J Balla for willing to serve on my committee and for his timely and insightful advice. Dr. Dieter Klatt has always been very welcoming to me in the group and Dr. Kamesh Bikkavilli has played the role of my mentor, from whom I could seek advice for my research as well as my career development. I learnt work-life balance from them, which helped me progress well. Dr. Sreedevi Avasarala has been a person who enjoyed my success and encouraged me to do more.

I thank Dr. David Kamp, Professor of Medicine at Northwestern University, and his lab members Seok Jo Kim and Paul Cherish for the collaboration and for providing the resources. It was a very fruitful

collaboration and a sheer joy to work with this group. Dr. Carol B Feghali, professor at the Medical University of South Carolina has been very kind to share the resources from IPF patients.

I thank Dr. Steven Kearney for his training on MRI/MRE, Brian Henry and Harish Slattery for being wonderful colleagues and friends over the years. I thank Eric Schmidt for the engineering support and his nice words of encouragement. I thank the people in Dr. Natarajan's lab for the experiences, which paved for a life-long learning. Mark Shaaya, Mounica Bandela, Panfeng Fu, Mrs. Lakshmi Natarajan have been very supportive colleagues in the lab and I cannot imagine my days in the lab without them. I would also like to thank Dr. Anantha Harijith, David Ebenezer, Alison Ha, Tanvi Sethi, all my mentees in the lab and members of the pulmonary division for the experiences.

Having been a very involved student on UIC, I cannot forget to acknowledge the impact all these leadership roles had on me. I had the privilege to work with some extraordinary individuals who have not only been able senior administrators on the campus, but also surprised me every time with their humility and openness to ideas from students like me. Dr. Pete Nelson, Dean of College of Engineering and also Dr. Fernando Testai, Associate professor, Department of Neurology and Rehabilitation have always been there for me, whenever I needed advice and guidance. Dr. Kenneth Brezinsky, Associate Dean for research, College of Engineering has been an incredible part of my experience and has been a mentor within and outside the Toastmasters club in the college of engineering.

I express my utmost thanks to my cousins Mr. Sreedhar Nadella and Dr. Rama Nadella for their never-ending support over the last three years and for being with me through all the tough times and for cherishing my strengths. I thank my friends Akshitha Reddy Thimmadi, Justin Sysol, Steffi Vinod and Cierra Hall for being charismatic and insightful friends.

TABLE OF CONTENTS

Chapter	Page Number
I Role of phospholipaseD in pulmonary fibrosis- Phospholipase D2 ablation alleviates pulmonary fibrosis by recuperating mitochondrial DNA damage and apoptosis	
1. Introduction:	01
1.1 Idiopathic Pulmonary fibrosis	01
1.1.1 Epidemiology of the disease	01
1.1.2 Etiology of IPF	01
1.1.3 Diagnosis of the disease	02
1.1.4 Current therapeutic strategies	03
1.2 Phospholipase D2	04
1.2.1 Isoforms of PLD	05
1.2.2 PLD2 in human disease	08
1.2.3 Role of PLD in fibrosis	08
1.3 Injury to the lung epithelium during IPF	09
1.4 Mitochondrial damage in the lung contributing to IPF	10
2. Materials and methods	12
2.1 Western blotting of lung tissues from of human subjects	12
2.2 Generation of wild type and <i>Pld2</i> ^{-/-} mice	12
2.3 Murine model of bleomycin-induced pulmonary fibrosis	13
2.3.1 Bronchoalveolar Lavage (BAL) fluid collection & analysis	15
2.3.2 Mouse lung tissue harvest and analysis	15
2.3.3 Histopathological analysis	16
2.3.4 Sircol assay	16
2.4 Cells and Reagents	16
2.5 Phospholipase D activity and expression	17
2.6 Western Blotting	17
2.7 Mitochondrial ROS generation	18
2.8 Mitochondrial DNA damage	18
2.9 Bronchial epithelial cell apoptosis	19
2.10 Statistical Analysis	19
3. Results	21
3.1 PLD expression in IPF and bleomycin-induced lung tissues	21
3.2 PLD expression in different cell types in IPF lung tissues	22
3.3 Genetic deletion of <i>Pld2</i> attenuates bleomycin-induced lung inflammation in mice	24
3.4 <i>Pld2</i> ^{-/-} mice are protective against bleomycin induced fibrosis	26
3.5 Genetic deletion of <i>Pld1</i> attenuates bleomycin-induced lung inflammation in mice	28

3.6	Genetic deletion of <i>Pld1</i> (<i>Pld1</i> ^{-/-}) attenuates bleomycin-induced lung fibrosis in mice	30
3.7	Bleomycin enhances PLD expression & activity, mt ROS in epithelial cells	31
3.8	PLD regulates mitochondrial ROS and antioxidant molecules in Beas2B	33
3.9	Inhibition of PLD attenuates bleomycin-induced mt DNA damage in lung epithelial cells	35
3.10	Inhibition of PLD attenuates bleomycin-induced epithelial cell apoptosis	36
4.	Discussion	39
4.1	Discussion	39
4.2	Conclusions	44
4.3	Future directions	46
II.	Fourier transform infrared imaging identifies biochemical changes in pulmonary fibrosis in a label-free manner	47
5.	Introduction	47
5.1	FTIR	47
6.	Materials and methods	50
6.1	Bleomycin induced PF in mice	50
6.2	Infrared micro spectroscopic imaging	51
6.3	Spectral pre-processing	51
6.4	K-means cluster analysis	51
6.5	Spectral analysis of normal and anomalous regions	52
6.6	PCA-LDA analysis	52
7.	Results and discussion	54
7.1	K-means analysis	54
7.2	Spectral analysis of fibrotic and non-fibrotic regions	58
7.3	Ratiometric analysis	59
7.4	Multivariate analysis	62
8.	Conclusion	65
8.1	Future directions	66
	SUMMARY OF THE STUDY	67
	BIBLIOGRAPHY	68
	APPENDIX	75
	VITA	77

LIST OF FIGURES

Figure	Page Number
1. Action of PLD	05
2. Isoforms of PLD	06
3. Mechanisms of IPF	10
4. Generation of <i>Pld1</i> ^{-/-} and <i>Pld2</i> ^{-/-} mice	12
5. Bleomycin-induced pulmonary fibrosis model	14
6. PLD2, but not PLD1 is upregulated in lung tissues obtained from patients with IPF and bleomycin-challenged mice	22
7. PLD2 staining in IPF lung tissue sections	23
8. Genetic deletion of PLD2 protects against bleomycin induced lung injury and inflammation	25
9. Genetic deletion of PLD2 protects against bleomycin induced fibrosis in mice	27
10. Genetic deletion of PLD1 protects against bleomycin induced lung injury & inflammation	29
11. Genetic deletion of PLD1 protects against bleomycin induced fibrosis in mice	31
12. Bleomycin enhances PLD activity, PLD2 protein expression and mitochondrial ROS generation in Beas2B cells	32
13. Inhibition of PLD1 and PLD2 activity attenuates bleomycin-induced mitochondrial ROS generation and modulation	34
14. Inhibition of mitochondrial superoxide generation and PLD attenuates bleomycin induced mtDNA damage in bronchial epithelial cells	36
15. Inhibition of mitochondrial superoxide generation and PLD attenuates bleomycin induced apoptosis in bronchial epithelial cells	37
16. Proposed mechanism of PLD2 in bleomycin-induced activation of mitochondrial ROS, mitochondrial DNA damage and apoptosis of bronchial epithelial cells	45
17. Array of representative tissue section examined by infrared microscopy	55
18. Non-hierarchical k-means cluster analysis depicting the histopathological regions of each lung across different groups	57
19. Average spectra in normal and anomalous regions of the lung	59
20. Ratiometric analysis of the IR spectra	61
21. PCA-LDA analysis could classify the different groups with varying stages of fibrosis	63

LIST OF ABBREVIATIONS OR NOMENCLATURE

Beas2B	Bronchial epithelial cells
BALF	Bronchoalveolar lavage fluid
FTIR	Fourier transform infrared
HRCT	High-resolution computerized tomography
IIP	Idiopathic interstitial pneumonias
IPF	Idiopathic pulmonary fibrosis
ILD	Interstitial lung disease
LDA	Linear discriminant analysis
MEA	monoethanolamine
PA	Phosphatidic acid
PLD	Phospholipase D
PCA	Principal component analysis
PF	Pulmonary fibrosis
ROS	Reactive oxygen species
UIP	Usual Interstitial pneumonia
DLCO	Diffusive capacity of the lung for Carbon monoxide

ABSTRACT

Idiopathic pulmonary fibrosis (IPF) is a pernicious lung disease characterized by scar formation and respiratory failure. This is due to dysregulated repair of the epithelial injury in the lung, which involves epithelial apoptosis, followed by activation of fibroblasts to mediate myofibroblasts, thereby leading to the deposition of the extracellular matrix in the lung. Currently there are only two FDA approved drugs for IPF; which do not cure the disease, but just slow the progression of disease, there is a need to identify new therapeutic targets for the disease. Phospholipase D (PLD), an important phospholipid metabolizing enzyme me involved in several pathophysiologies, catalyzes the hydrolysis of phosphatidylcholine (PC), generating phosphatidic acid (PA) and choline. In addition to PC, PLD also hydrolyzes other phospholipids such as phosphatidylethanolamine (PE) and cardiolipin (CL). PLD mediated PA generation is involved in regulation of various cellular processes including cell survival, cell migration, cell proliferation, differentiation, cytoskeletal changes, membrane trafficking, and autophagy.

Previous studies have shown that PLD has a role in cardiac and hepatic fibrosis, but the mechanism(s) by which PLD mediates fibrosis has not been identified. This study is aimed at delineating the PLD signaling mechanism in IPF to identify new therapeutic targets. Of the two PLD isoenzymes, PLD1 and PLD2, the protein expression of PLD2 was up-regulated in bleomycin induced pulmonary fibrosis (PF), and PLD2 deficient mice (*Pld2*^{-/-} null) were protected against bleomycin induced lung inflammation and fibrosis, thereby establishing the role of PLD in IPF. To further understand how PLD mediates epithelial injury during IPF, bronchial airway epithelial cell line (Beas2B cells) was used, and *in vitro* studies showed that bleomycin challenge led to enhanced PLD activity in the cells; led to generation of mitochondrial reactive oxygen species (ROS) and apoptosis in Beas2B cell line. Further, inhibition of PLD2 in Beas2B cells attenuated bleomycin induced mitochondrial DNA damage and epithelial cell apoptosis. Thus, we

identified that reducing bleomycin-induced PLD activity will lessen mitochondrial ROS generation, thereby leading to less mitochondrial dysfunction and eventually less apoptosis of the epithelial cells. This study identifies PLD to be a promising therapeutic target in IPF.

In addition to identifying new therapeutic targets, the current research study is focused on developing new diagnostic techniques for IPF. Fourier Transform Infrared (FT-IR) imaging technique is a label-free, non-destructive approach to detect histopathological changes in the tissue. IR spectra has been acquired from the lungs from bleomycin challenged mice harvested at different time-points. The biochemical changes that occur in the lung tissue during the development of fibrosis can be detected by this technique, based on the spectral profile acquired. The spectral data obtained is subjected to unsupervised cluster analysis which classifies it into based on the histopathological states. The ratio of absorption of spectral ratios gives the collagen map, glycosylation and structural deformations across the lung tissue. Linear discriminant analysis was done to classify and identify the extent of disease progression. This novel technique gives the biochemical information across the entire lung tissue and enables diagnosis of the disease in a label-free manner.

Chapter I: Role of PhospholipaseD in pulmonary fibrosis-Phospholipase D2 ablation alleviates pulmonary fibrosis by recuperating mitochondrial DNA damage and apoptosis

1. INTRODUCTION

1.1 Idiopathic pulmonary fibrosis:

Idiopathic pulmonary fibrosis (IPF) is a detrimental lung disease which is characterized by scar formation and respiratory failure, and eventually death. The lung interstitium is disrupted due to the scar formation, thereby making the lung stiff and hard to expand which results in limited oxygen uptake into the bloodstream. IPF comes under the broad spectrum of interstitial lung diseases, which encompasses over 200 diffuse parenchymal lung disorders [1], that mainly impact the lung interstitium, which is the tissue and the space around the lung alveoli [2].

1.1.1: Epidemiology of the disease:

The worldwide statistics by 2014 show that it affects about 5 million people. Over the globe about 13-20 people are affected by IPF for every 10,000 people. It is prevalent over 130,000 people in the US [3], where about 30,000-40,000 cases are newly diagnosed each year. The disease is predominant in elderly men.

1.1.2: Etiology of IPF:

The term 'idiopathic' means unknown cause. It might occur due to various reasons like familial causes, genetic causes, occupational exposure, radiotherapy, chemotherapy, bacterial and viral infections [4]. Occupational exposure to silica dust, asbestos fibers, grain dust, hard metal dusts, coal dust, bird and animal droppings during mining, construction or farming and several other irritants and sustained

exposure to bacterial or viral loads leads to the development of pulmonary fibrosis. Radiation therapy to treat any lung disorders or breast disorders also leads to radiation-induced damage to the lungs, based on the dosage and extent of exposure of radiation to the lungs. Lung fibrosis also occurs due to various chemotherapeutic agents (like bleomycin, cyclophosphamide, methotrexate), antibiotics (nitrofurantoin, ethambutol), anti-inflammatory drugs (sulfasalazine and rituximab) and cardiac medication like amiodarone employed to treat irregular heartbeats [5]. Several pre-existing medical conditions like scleroderma, pneumonia, sarcoidosis, dermatomyositis, Systemic lupus erythematosus, Polymyositis, Rheumatoid arthritis, mixed connective tissue diseases also contribute to IPF. IPF is more prevalent with increased aging and more prevalent in men than in women. Smoking is one of major causes of IPF and continued smoking will lead to worsened survival of IPF [6]. In some cases, genetic factors contribute to IPF [7], like changes in several genes including Muc5B.

There are also other comorbidities associated with IPF like Gastroesophageal reflux disease, lung cancer, pulmonary hypertension, chronic obstructive pulmonary disease, pulmonary embolism, diabetes, ischemic heart disease, and obstructive sleep apnea [8]. Looking at these comorbidities can provide further clues that help in the diagnosis of IPF.

1.1.3: Diagnosis of the disease:

Patients with IPF show symptoms only during the advanced stages of disease. They have shortness of the breath not only during exercise, but also during rest; dry hacking cough; clubbing of fingers which is rounding and widening of the fingers and toes; inadvertent and gradual weight-loss. A multidisciplinary approach employing pulmonologists, radiologists and pathologists is needed for the diagnosis of IPF. High-resolution computerized tomography (HRCT) of the lungs examines the radiological features of the lung and offers the initial detection of IPF based on the presence of Usual Interstitial Pneumonia (UIP) pattern of IPF. Lung function tests like lung volumes, spirometry, diffusing capacity of the lung for carbon

monoxide (DLCO), pulse oximetry tests to determine the amount of oxygen in the blood, arterial blood gas test, six-minute walking tests are used to identify the progression of the disease.

Further, lung biopsy is needed to validate the presence of IPF, followed by histopathological analysis to demonstrate the characteristic features and exclude alternative diagnoses. Lung biopsy can be done by either video-assisted thoracoscopy using endoscope, bronchoscopy or thoracotomy. Distinctive honeycombing patterns are seen in some cases of IPF, which is the scar deposition in the interstitial spaces of the lung, in addition to collapse of the alveolar spaces into large cysts[9].

1.1.4: Current therapeutic strategies:

Non-pharmacological treatment: Pulmonary rehabilitation is the ‘first line of therapy for IPF’ wherein patients do structured exercise, acquire knowledge about proper breathing techniques and usage of oxygen [3]. It has several benefits as it improves the lung function, and reduction in symptoms, thus improving the quality of life (QoL). Supplemental oxygen therapy is most commonly done in patients with IPF[10], when the oxygen levels are low and it’s helps in reducing the symptoms for IPF. Lung transplantation is done in patients with IPF after the lung has collapsed, however, the survival rate is only three to five years, even after the transplantation[11].

Pharmacological treatment: Nintedanib and perfenidone are the only two FDA approved drugs for the treatment of IPF [12]. These drugs only slow the progression of disease, but do not cure the disease. The only curative intervention is lung transplantation, but nevertheless the 5-year survival rate of patients who undergo lung transplantation is only 45% [13]. This lack of attractive treatment options necessitates development of new agents; however, the study of new therapeutic modalities depends on reliable, accurate, and sensitive methods for diagnosis and disease monitoring.

1.2 Phospholipase D:

Phospholipase D (PLD) is an important phospholipid metabolizing enzyme that hydrolyzes phosphatidylcholine (PC) or other glycerophospholipids to phosphatidic acid (PA) and choline or a water-soluble base [14] as shown in **Figure.1**. PA acts as a second messenger and regulates several key biological processes including apoptosis, cytoskeletal organization, cell morphogenesis, membrane biogenesis and vesicular trafficking [15]. Also, PA is catabolized to diacylglycerol (DAG) by lipid phosphate phosphatases [16] or lysophosphatidic acid (LPA) by PA specific phospholipase A1 or A2 [16] in cells. Both DAG and LPA are signaling lipid molecules; DAG activates PKC [17] and LPA signals via G-protein coupled LPA₁₋₆ receptors in mammalian cells. Thus, activation of PLD and generation of PA is central to cellular signal transduction under normal and pathological conditions. PLD serves as a transmembrane signal transduction protein which is activated by hormones, neurotransmitters and growth factors [18]. PLD is also a transphosphatidylase that generates phosphatidylalcohols by using short-chain primary alcohols (methanol, ethanol, butanol and propanol) as an acceptor instead of H₂O (competitive nucleophiles).

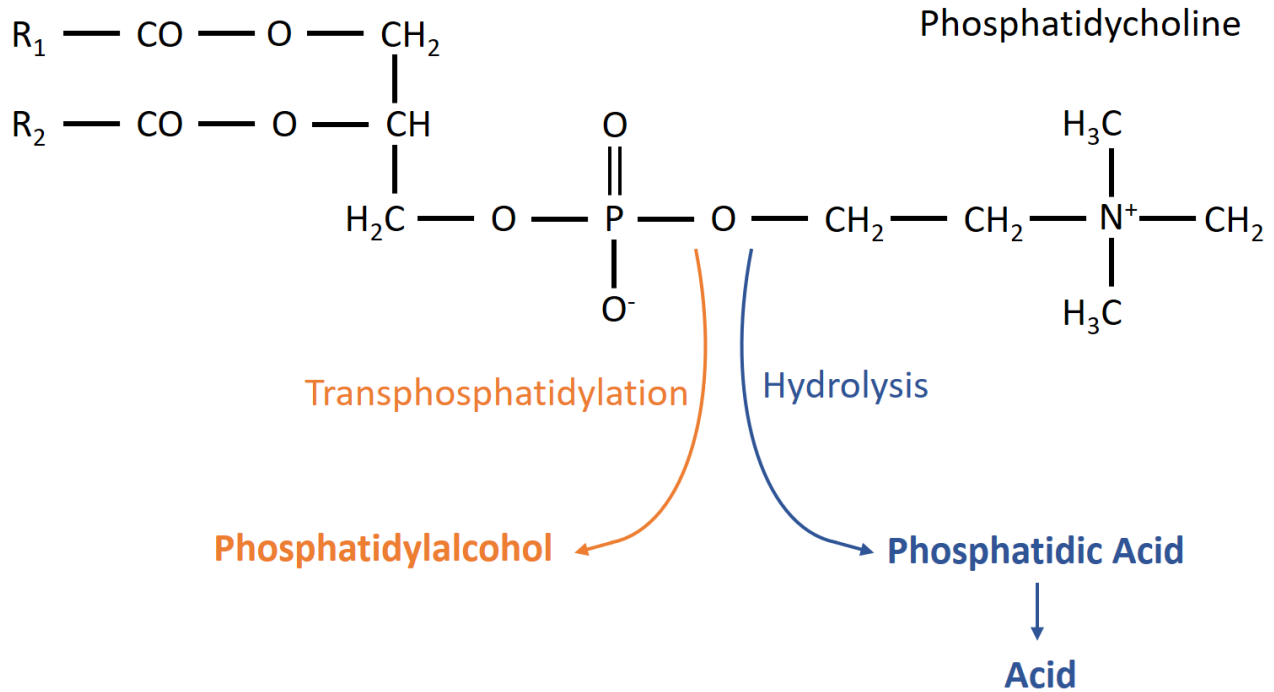


Figure1: Action of PLD: Phosphatidylcholine is hydrolyzed by PLD to generate PA, an important second messenger. However, in the presence of alcohols, PC undergoes transphosphatidylation to generate phosphatidylalcohol [19]

1.2.1 Isoforms of PLD:

There are six major isoforms of PLD (**Figure. 2**) among which PLD1 and PLD2 have been identified to play a key role in several cell signaling mechanisms [20] and involved in several pathophysiological processes including but not limited to cancer, cardiovascular disease, acute lung injury, infectious diseases and neurodegenerative disorders [21]. Of the six isoforms, only PLD1, PLD2 and PLD6 (mito PLD) exhibit activity.

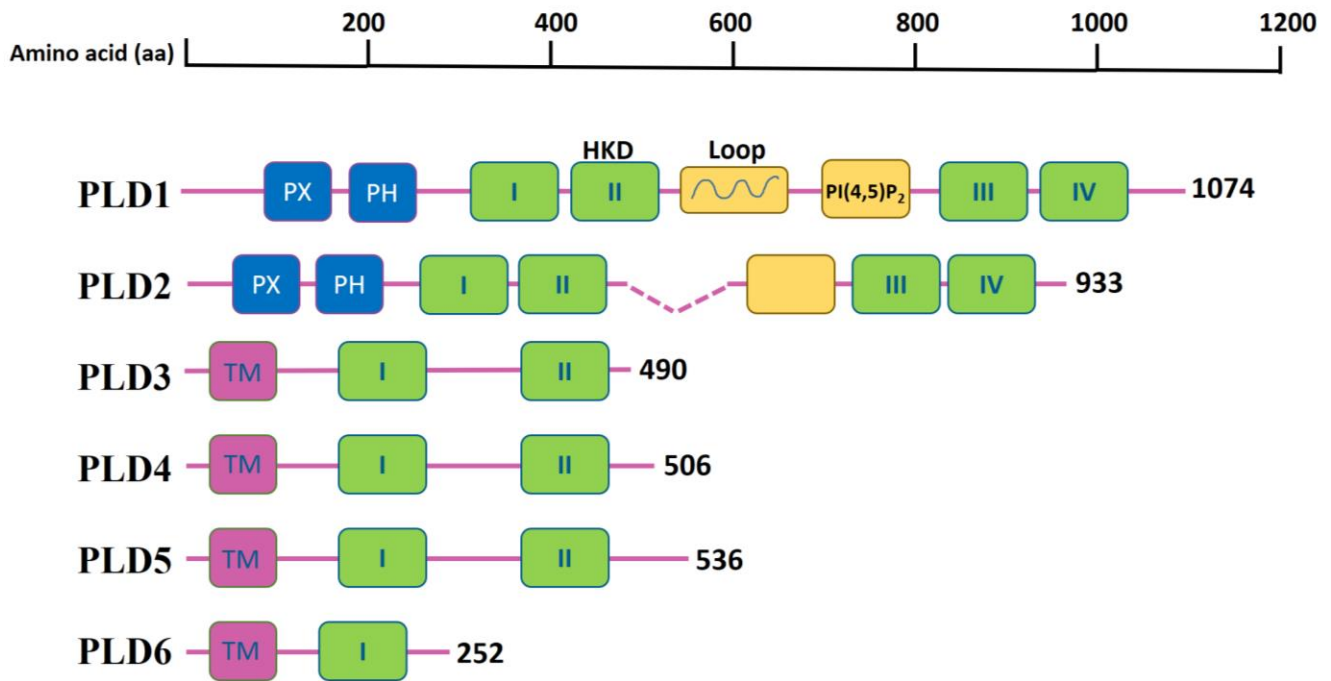


Figure2: Isoforms of PLD

PLD enzymes have four conserved regions (I-IV), which includes the catalytic domains (II & IV) having the HxxxxDxKx sequence with Histidine (H), any amino acid (x) and lysine (K) and aspartic acid (D). Phox consensus sequence (PX), the plekstrin homology (PH) domain are the other conserved regions of the PLD genes along with the PI_{4,5}P₂ binding site. PX domain binds to phosphatidylinositol (PtdIns) and its phosphates and other PIPs and mediates protein-protein interactions with regulatory proteins like dynamin and Grb2. PH domain is mainly involved in localization of the protein and plays a role in the intracellular trafficking by the endocytic pathway. PLD1 has an additional conserved loop region that is not found in PLD2. This loop region regulates PLD1 activity by serving as negative regulatory element

as indicated by the increased basal PLD activity by three-fold upon deletion of the loop region from PLD1. PLD1 has low basal activity which is regulated by Arf, Rho and Ral GTPases and protein kinase C (PKC) [22]. PLD2, on the other hand has higher basal activity and is regulated by Arf and PKC in mediating a wide range of protein-protein interactions [23].

The PLD1 and PLD2 isoforms have distinct subcellular localization. Basally, PLD1 is present on perinuclear membranes, Golgi complex, endoplasmic reticulum (ER), endosomes and lysosomes [24]. PLD1 translocate to the plasma membrane upon stimulation, otherwise it is involved in the budding and fusion of trans-Golgi-derived subcellular localization. PLD2 on the other hand is mainly localized in the plasma membrane, and involved in signal transduction; and also present in the cytosol and sub-membranous vesicular compartments [25].

PLD3 is an integral ER transmembrane protein that lacks PX and PH domain and has no catalytic function though it has a pair of HDK domains[26] and has been associated with survival and cell differentiation [20]. PLD3 has been found to play a role in Alzheimer's disease [27] and myotube formation[26]. Like PLD3, PLD4 is also a HKD motif-carrying non-catalytic, transmembrane glycoprotein that is localized in the plasma membrane, endoplasmic reticulum and Golgi apparatus [28].

PLD4 has been found to be involved in tumor associated macrophage activation [29], microglial activation which impacts myelination during brain development [30], systemic sclerosis [31] and kidney fibrosis [32]. PLD5 has a putative transmembrane domain instead of PX and PH and has been found to be associated with autism [33]. PLD6 acts as an endonuclease that generates the 5 ends of PIWI-interacting RNAs (piRNAs)[34] and also involved in spermatogenesis [35]. Mitochondrial PLD has been characterized in mammalian cells and has no similarity to the typical PLD family. It has a single PLD catalytic HxKxD motif and generates PA by using cardiolipin as the substrate [36], which facilitates mitochondrial fusion.

1.2.2 PLD2 in human disease:

Over the recent years, the availability of genetically engineered knock-out mice and isoform-specific inhibitors to specifically block PLD1 and PLD2 has enabled a better understanding of the mechanism(s) behind the involvement of PLD1 and PLD2 in various human pathophysiologies. PLD1 deficiency blunts immune responses and has found to play an important role in several autoimmune diseases, including multiple sclerosis [37]. PLD2 was found to be responsible for the uptake of influenza virus by endocytosis route and permits viral escape from innate immunity, whereas PLD1 played a vital role in egress, assembly and budding of the virus [38].

PLD1, 2 and 3 are the important isoforms involved in brain function and neurodegenerative diseases like Alzheimer's disease [39]. Enhanced PLD activity, expression of specific isoforms and has been implicated in several cancers including that of lung, liver, colon, brain, breast, pancreatic, prostate, renal and ovarian cancer [40]. This is due to the involvement of PLD isoforms in tumorigenesis and several cellular mechanisms mediating cancer like cell survival, migration and proliferation [41].

1.2.3 Role of PLD in fibrosis:

PLD1 was found to induce hepatic stellate cell activation that plays a prominent role in liver fibrosis. Treatment of mice with monoethanolamine (MEA) was found to reduce the severity of Dimethylnitrosamine-induced liver fibrosis [42]. PLD has been found to play a crucial role in cardiac fibrosis as blocking PLD using MEA reduced left-ventricular fibrosis and hypertrophy [43] in addition to preventing myocardial stiffening and pulmonary congestion. Reduction of PLD4 was found to impact several fibrogenic mechanisms that included increase in antifibrotic cytokines, neutrophil elastase that degrades ECM proteins, reduction in TGF- β and MAPK signaling [32]. Thus, PLD4 was found to be therapeutic target that could reverse kidney fibrosis. Bleomycin, a potent inducer of lung fibrosis was

found to induce PLD activity in lung microvascular endothelial cells in a redox sensitive manner [44]. In this study we have investigated the role of PLD in lung epithelial cells, since it's the first line of injury during any insult to the lung. Both the PLD isoforms have been implicated to regulate several key signaling pathways [45].

1.3 Injury to the alveolar epithelium during fibrosis:

The epithelium is the first line of injury to the lung during any kind of insult caused by pollutants, cigarette smoke and irritants. Dysregulated epithelial repair followed by the fibrotic process leads to irreversible damage to the lung. The injured epithelium releases pro-inflammatory and profibrotic cytokines which further activate the fibroblasts in the lung. These fibroblasts further proliferate and differentiate into myofibroblasts leading to the deposition of extracellular matrix components contributing to fibrosis [46]. This trans differentiation of epithelial cells into fibroblasts is termed as epithelial to mesenchymal transition (EMT) and is one of the important mechanisms that mediate the fibrotic mechanisms in the development of pulmonary fibrosis [47].

Also, epithelial damage and apoptosis is one of the prominent features of IPF. The inflammatory cascade by itself was not sufficient to induce pulmonary fibrosis, and epithelial cell apoptosis was imperative for the progression of bleomycin induced PF.¹

Hyperplastic epithelium, sizable cuboidal cells protruding into the alveolar lumen, was seen in lung tissues of IPF patients in contrast to the normal epithelium lining the lung which are thin, elongated and flat cells. The hyperplastic alveolar and bronchial epithelial cells were found to undergo apoptosis, and this hinders rapid re-epithelialization in the lung. This development of scanty and impaired re-epithelialization leads to fibrogenesis and thus fibrosis.

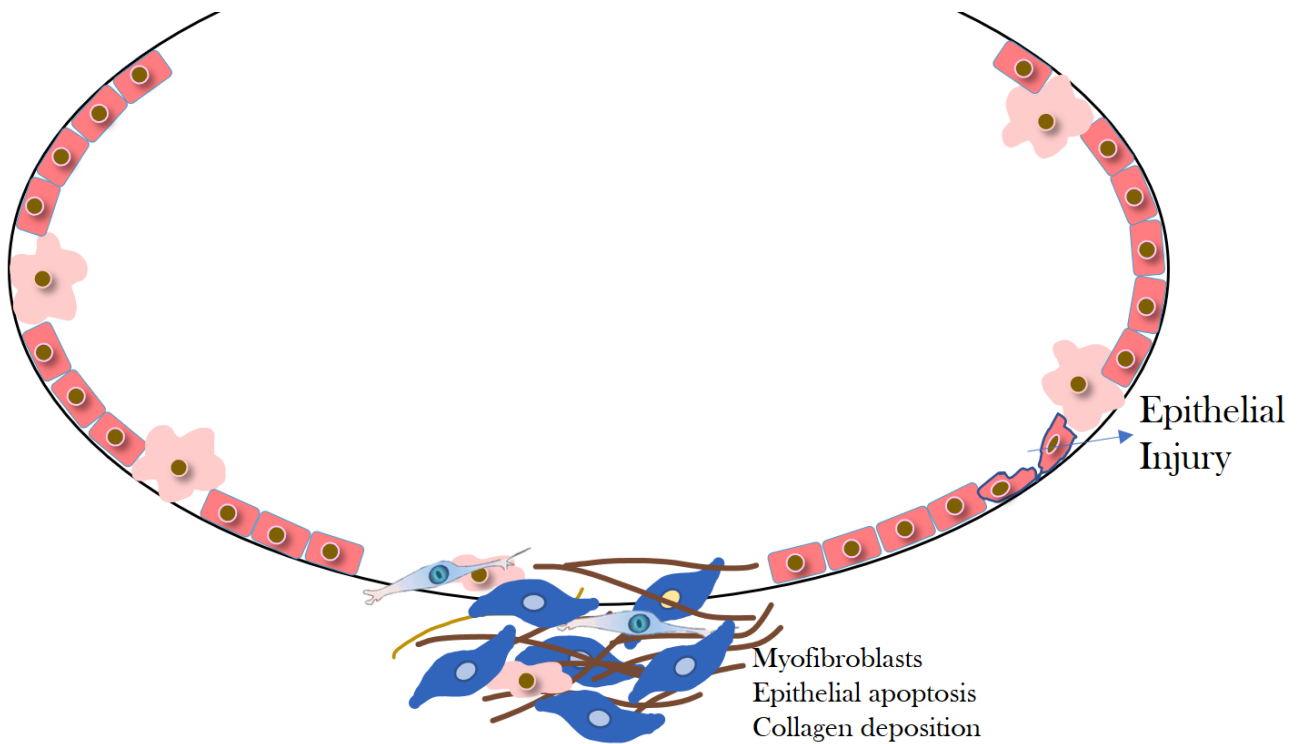


Figure 3: Mechanisms of IPF: Honeycombing can be seen predominantly in the fibrotic lung. These regions have cytokines and chemokines released from the damaged epithelial cells; activated fibroblasts transformed to myofibroblasts and the extracellular matrix secreted that makes the lung stiff.

1.4 Mitochondrial damage in the lung contributes to IPF

Oxidative stress is one of the important mechanisms involved in the development and progression of IPF [46]. Mitochondrial (mt) DNA damage causing mitochondrial dysfunction can lead to epithelial apoptosis which is predominant in IPF. MtDNA is sensitive to damage, almost by 50-fold in comparison with nuclear DNA, one of the factors being the proximity of mtDNA to electron transport chain (ETC). The other factors contributing to the sensitivity of mtDNA to damage is the absence of a histone protective

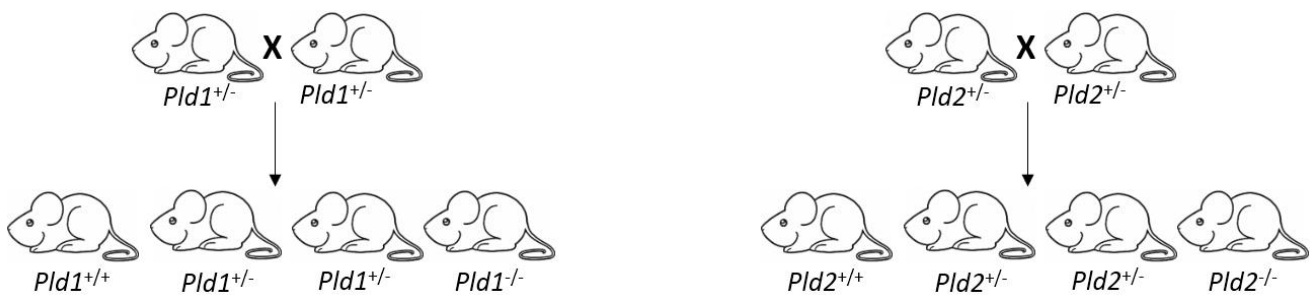
shield around the mtDNA and deterrent DNA repair mechanisms in mitochondria [48]. The human mitochondrial genome is a circular DNA molecule of approximately 16 kilobases, and it encodes 37 genes, out of which 13 genes are for subunits of respiratory complexes I, III, IV and V; 22 genes for mitochondrial tRNA; and 2 genes for rRNA. Two to ten copies of DNA are present in each mitochondrion. Cell has approximately 100 copies of mtDNA and this encodes about 3% of mitochondrial proteins, which are essential for regulating mtDNA-associated proteins, like 8-oxoguanine glycosylase (OGG1), mitochondrial aconitase (ACO2), mitochondrial transcription factor A (Tfam), and others [49]. Previous studies by Dr. Kamp and his group at Northwestern University, Chicago have shown alteration of several mitochondrial proteins in IPF such as reduced expression of Sirtuin 3 (Sirt3), which detoxifies mt ROS [50]. Further in IPF lungs, enhanced acetylation of MnSOD was also observed, which leads to inactivation of the antioxidant defense mechanism in IPF lungs [49].

2. MATERIALS AND METHODS

2.1 Western blotting of lung tissues from of human subjects: Lung tissue lysates from normal and IPF patients undergoing biopsy were obtained from Dr. Carol Bostwick-Feghali at the Medical University of South Carolina, with a collaborative agreement. Specimens of IPF lung tissues were obtained from patients who underwent lung transplantation, and normal lung tissue specimens were obtained from donors whose lungs were not used for transplant surgery at the University of Pittsburgh Medical Center, under a protocol approved by the University of Pittsburgh Institutional Review Board, and from normal lung tissue obtained from organ donors. Protein concentration was determined from the lung tissue homogenates and equal amount of proteins were probed with PLD1, PLD2 (1:1000 dilution, Cell Signaling, Danvers, MA) and β -Actin (1:10,000 dilution, Millipore Sigma, St. Louis, MO) antibodies.

2.2 Generation of *Pld1*^{-/-} and *Pld2*^{-/-} mice:

PLD1 and PLD2 heterozygous mice were obtained from Dr. Gilbert Di Paolo, Columbia University. The heterozygous mice were intercrossed to obtain homozygous mice. Multiplex PCR of tail snip DNA was used to genotype the mice.



4: Generation of *Pld1*^{-/-} and *Pld2*^{-/-} mice

The following primers were used for genotyping of *Pld1*^{+/+}, *Pld1*^{+/-} and *Pld1*^{-/-} mice:

WT allele amplification:

PLD1-047 GAAGGGATAGGAAAGTCCAGG

PLD1-027R GGAGCCCAATAGGTAGAGTG

Mutant allele amplification:

PLD1-049 GGGTGGAAAGAGAACCCATAG

PLD1-027R GGAGCCCAATAGGTAGAGTG

The following conditions were used:

1. Initial denaturation 95°C for 3 min;
2. Amplification (35 cycles)
94°C for 30sec
58°C for 30sec
72 °C for 50sec;
3. Final elongation 72 °C for 10 min.

PCR amplification for WT gives a band at 450bp, for *Pld1*^{-/-} is 458bp and for *Pld1*^{+/-} 450 and 458bp. This would distinguish *Pld1*^{+/+} mice from *Pld1*^{-/-} mice.

The following primers were used for genotyping of *Pld2*^{+/+}, *Pld2*^{+/-} and *Pld2*^{-/-} mice:

PLD2-003 GGGAATCTGAGGCTTCAAGACTGGG

PLD2-013 GGACTGGGTGCAGCTGGACC

PLD2-045R GCTGGTGT TTTGAGGATGCTTG

The following conditions were used:

1. Initial denaturation 95°C for 3 min;
2. Amplification (35 cycles)
94°C for 30sec
60°C for 30sec
72 °C for 45sec;
3. Final elongation 72 °C for 10 min.

PCR amplification for WT gives a band at 579bp, for *Pld2*^{-/-} is 521bp and for *Pld2*^{+/-} 579 and 521bp. This would distinguish *Pld2*^{+/+} mice from *Pld2*^{-/-} mice.

2.3 Murine model of bleomycin-induced pulmonary fibrosis:

Several animal models have been used to study IPF, each of them with their own advantages and disadvantages in terms of their replicability to human IPF. Some of these models include challenging mice

with Asbestos , bleomycin, radiation or fluorescein isothiocyanate, and transgenic models wherein cytokines are overexpressed, and humanized model of pulmonary fibrosis [51]. Many of these animal models are different from human IPF in their own way. Despite the fact that there is minimal inflammation in human IPF, the bleomycin model is predominantly an inflammation model; however, , offers several advantages like mimicking the mechanistic aspects of the disease including hyperplastic epithelial cells, EMT, and TGF- β -induced fibroblast differentiation. [52]. Infusion of bleomycin induces ROS generation in the lung [44], which triggers lung inflammation and injury and stimulates deposition of extracellular matrix proteins and collagen by 21 days post-bleomycin challenge. . Although bleomycin-induced pulmonary fibrosis model is one of the well-characterized models to study pulmonary fibrosis, the fibrosis resolves after 28 days of bleomycin challenge and therefore not useful to study long term fibrosis in the lung.

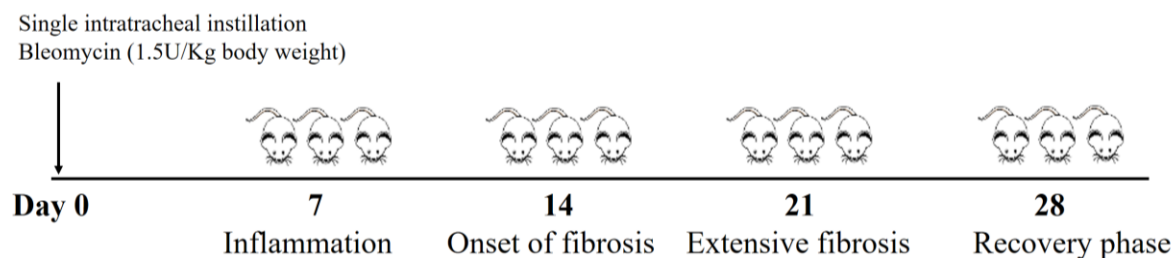


Figure 5: Bleomycin induced pulmonary fibrosis model

Wild type, *Pld1*^{-/-} and *Pld2*^{-/-} mice of about 8-12 weeks were used for experiments. The mice were anesthetized with 100 mg/kg ketamine + 5 mg/kg xylazine IP and bleomycin, obtained from Hospira Inc. (Lake Forest, IL) (1.5U/Kg) was instilled intratracheally to the mice, based on the weight of the mice with a maximum volume of 50µl. All experiments were performed in accordance with ACC approved protocols. The mice were euthanized after 0, 7, 14, 21, 28 days of post-bleomycin injection for analysis.

2.3.1 Bronchoalveolar lavage fluid collection and analysis:

Bronchoalveolar lavage (BAL) fluid was collected by intratracheal injection of 1ml of PBS, spun at 500g for 20 minutes at 4°C, supernatant was collected, and the pellet was used for total cell count analysis. The supernatant was further spun at 10,000g for 10 min at 4°C, and stored as BAL fluid at -80°C for analysis of cytokines, protein concentration and hydrogen peroxide. Protein concentration of the BALF fluid, a measure of the alveolar permeability, was measured using BCA protein assay kit (Pierce Thermo scientific, Rockford, IL). Cytokine levels in the cell-free BAL fluid samples were measured using ELISA kits (Peprotech, NJ), according to the manufacturer's instructions. The pellets from first step of centrifugation were resuspended in 200µl PBS and total cell counts were done using TC20™ automated cell counter from Biorad. 20µl aliquots were spun onto microscope slides and stained using Diff-Quik stain set (Dade-Behring, Newark, DE) for differential cell counts.

2.3.2 Mouse lung tissue harvesting and analysis:

After BAL fluid collection, the right lung of the mouse was excised, snap-frozen in liquid nitrogen and stored at -80°C. The left lung was fixed with formalin for histological analysis. The frozen lung tissue was diced, and lung homogenates were prepared in 350µl of RIPA buffer containing protease and phosphatase inhibitors. The homogenized samples were sonicated and spun at 10,000g at 4°C for 10 minutes to remove cell debris, and the clear supernatant of the lung homogenate samples were used for total protein.

2.3.3 Histopathological analysis:

Formalin fixed lung tissues were embedded in paraffin and later sectioned onto glass slides (3-5 μ m). The lung tissue sections were stained with Hematoxylin & Eosin (H&E) to assess for lung injury and with Masson's trichrome staining to assess for collagen deposition in the lung, which is a marker of fibrosis. Lung injury was scored from the H&E staining on the basis of the report from the official workshop report by the American Thoracic society that was written to distinguishing the features of acute lung injury [53]. The extent of lung fibrosis was determine by evaluating the Ashcroft score as done previously [54]. The mean score from each lung section was computed after observing and assessing multiple fields from each lung section separately and averaging them in a blinded manner.

2.3.4 Sircol assay:

Acid-soluble collagen levels in the lung tissue were measured using Sircol soluble collagen Assay (Biocolor Ltd., Newtownabbey, Northern Ireland). This technique has been widely used to determine the new synthesized soluble collagen (in case of remodeling of the extracellular matrix during the repair and regeneration process), that is recovered from soft mammalian tissue, including the lungs. On the other hand, the insoluble collagen is the abundant, residual collagen present in mammals to retain biophysical function and shape. The right lung homogenate was mixed with Sircol dye and rotated overnight at 4°C. They were cleared by centrifugation at 12,000g for 15 min. The pellet was washed with acid salt wash reagent provided by the supplier and finally suspended in alkali reagent. The readings were taken at 555nm and the values were presented as micrograms of acid-soluble collagen levels per right lung.

2.4 Cells and reagents:

Beas2B cells were purchased from ATCC (Manassas, VA) and cultured in DMEM (Corning Inc., Corning, NY) medium supplemented with 10% FBS (Millipore Sigma, St. Louis, MO) and 1%

Pen/strep. Primary HBEPs (passage 2) were purchased from Lonza (Rockville, MD) and cultured in serum free basal essential growth medium (BEGM) and supplemented with growth factors provided by the supplier. Cells were incubated at 37 °C in 5 % CO₂ and 95 % air to ~ 80 % confluence and subsequently propagated in 100-mm or 35-mm fibronectin-coated dishes. All experiments were carried out between passages 3 to 6. PLD1 inhibitor, VU0155069 and PLD2 inhibitor, VU 0364739 were obtained from Cayman Chemical (Ann Arbor, MI).

2.5 Phospholipase D activity and expression: Phospholipase D (PLD) activity was measured using Amplex Red Phospholipase D Assay Kit (ThermoFisher Scientific, Waltham, MA). The cell lysates were incubated with the reaction mixture for 37°C in the dark. PLD activity present in the cell lysates cleaves the lecithin (phosphatidylcholine) substrate in the reaction mixture to produce choline and phosphatidic acid. The choline oxidase that is present in the reaction mixture oxidizes choline to betanine and H₂O₂. The kit indirectly measures PLD activity by measuring the fluorescence intensity of the resorufin resulted from reaction with H₂O₂. The fluorescence was measured at 540nm. The expressions of PLD1 and PLD2 in cell lysates and tissue homogenates were determined using western blotting from cell lysates with and without bleomycin challenge.

2.6 Western blotting: The lung tissue or cell lysates were subjected to SDS-PAGE on a 10% or 4-20% gel pre-cast gel (Invitrogen, Carlsbad, USA) run at constant voltage (225 V) and transferred to nitrocellulose membranes (Bio-Rad, Hercules, CA). The membrane was blocked for 1h at room temperature in blocking buffer (Tris-buffered saline + Tween 20 with 1% BSA) to reduce non-specific binding. The membrane was then incubated with the respective primary antibody overnight. The primary antibodies used were PLD1(#3832), PLD2 (#13891), PARP (#9542), and Caspase-3 9#9662) (1:1000 dilution Cell Signaling, Danvers, MA); β -Actin (1:10,000 dilution, #A5441 MilliporeSigma, St. Louis, MO); AcMnSOD K68 (1:1000 dilution, #137037 Abcam, Cambridge, UK), SOD (1:1000 dilution, #

18504 Santa Cruz, Dallas, TX). After four 10-min washes with TBST, membranes were incubated (1 h) with the respective secondary antibody in TBST containing 1% BSA. Species specific horseradish peroxidase secondary antibodies were obtained from Biorad (Hercules, CA). The membranes were rinsed again four times with TBST for ten minutes each time, and the bands were detected using Supersignal luminol enhancer (Perbio Science UK Ltd., Cheshire, UK) followed by exposure to blue-light-sensitive X-ray film (Hyperfilm; Amersham Biosciences UK Limited, Little Chalfont, UK). Equal protein loading was verified by re-probing membranes with anti- β -actin antibody. The relative intensities of protein bands (relative density units) were quantified by scanning densitometry using ImageJ software (Molecular Dynamics, Sunnyvale, CA).

2.7 Mitochondrial ROS generation: Mitochondrial superoxide generation in Beas2B cells upon bleomycin challenge was determined by using MitoSOXTM red mitochondrial superoxide indicator (ThermoFisher Scientific, Waltham, MA). The effect of inhibiting PLD activity on bleomycin induced superoxide generation was evaluated by pre-incubating the cells with 250 nM PLD1 inhibitor (VU0155069), 500nM PLD2 inhibitor (VU 0364739) or a combination of both the inhibitors for 3 h prior to bleomycin challenge (1 h). After bleomycin challenge, cells were loaded with 5 μ M MitoSOXTM reagent for fifteen minutes at 37°C and then washed two times in phenol-red free media. The cells were examined under Nikon Eclipse TE 2000-S fluorescence microscope and pictures were captured on a Hamamatsu digital charge-coupled device camera (Japan) using a 60X objective lens.

2.8 Mitochondrial DNA damage: We assessed mitochondrial and nuclear DNA damage by Q-PCR as we have previously described [55]. Genomic DNA, including both nuclear and mitochondrial DNA (mtDNA), was extracted using Qiagen Genomic-Tip 20G and Qiagen DNA Buffer Set (Qiagen, Gaithersburg, MD, USA) and was assessed by Q-PCR (Thermo Fisher Scientific, Waltham, MA). DNA was quantified by Pico-green (Thermo Fisher Scientific) using the FL600 Microplate Fluorescence Reader

(Tecan, Männedorf, Switzerland) parameters excitation and emission wavelengths 485 and 530 nm. Data obtained from the small fragments was subsequently used to normalize the results of the mitochondrial long fragment. To compare the levels of DNA lesion in each tested region of the mitochondrial genome, two mtDNA fragments of different lengths (long fragments ranging from 972 to 1037 bp and small fragments from 54 to 87 bp, respectively), located in the same mitochondrial genomic region were used. The number of mitochondrial lesions was calculated by using the following equation: $D = (1 - 2^{-(\Delta_{\text{long}} - \Delta_{\text{short}})}) \times 10,000$ (bp)/size of the long fragment (bp). The effect of PLD2 inhibition on mtDNA damage was evaluated by pre-incubating the cells with 250nM PLD1 inhibitor (VU0155069) and 500nM PLD2 inhibitor (VU 0364739) and a combination of both for 3hr. In separate experiments, the cells were also pre-incubated with mito TEMPO three hours prior to bleomycin challenge (24 h), to study the impact of blocking mitochondrial superoxide on mt DNA damage.

2.9 Bronchial epithelial cell apoptosis: The effect of inhibiting PLD activity on bleomycin induced apoptosis was evaluated by pre-incubating the cells with 250nM PLD1 inhibitor (VU0155069), 500nM PLD2 inhibitor (VU 0364739) or a combination of both the inhibitors for 3 h prior to bleomycin challenge (24 h). The cell lysates were subjected to Western blotting for Caspase-3, PARP, cleaved of Caspase-3 and PARP fragments, which were markers of apoptosis. Another alternative approach to determine apoptosis was by flow cytometry analysis using FITC Annexin V Apoptosis detection kit from BD Biosciences (San Jose, CA). After bleomycin treatment for 24 h, the cells were collected using dissociation buffer, washed with ice cold PBS. The cells were suspended in 300 μ l binding buffer prior to being loaded with 10 μ L of Annexin V-FITC, then gently vortexed and incubated for 10 min at 4 C in the dark. 3 μ L of PI was added to each tube for another 5 min at 4 $^{\circ}$ C in the dark. The cells were evaluated for annexin V-FITC and PI binding by Beckman Coulter's Gallios flow cytometer.

2.10 Statistical Analysis: Experimental results are expressed as means \pm SD of triplicate values from three independent experiments. All results were subjected to statistical analysis using one-way ANOVA and, whenever appropriate, analyzed by Student-Newman-Keul's test $p < 0.05$ was considered statistically significant.

3. RESULTS

3.1 PLD expression in IPF and bleomycin-induced lung tissues:

Lung tissues from ten normal subjects and ten IPF patients were subjected to Western blotting. It was found that the PLD2 expression was upregulated in the lung homogenates of IPF patients than those of control subjects (**Figure.6A and 6B**), as quantified in 6C.

The mice were given bleomycin (1.5U/Kg) intratracheally and the mouse lungs were harvested on Day 14. The whole lung tissue lysates were subjected to immunoblotting for PLD1 and PLD2. It was observed that there was an increase in protein expression of PLD2 in lung tissue lysates of bleomycin-challenged mice than control mice, but there was no change in the protein expression of PLD1, as seen in **Figure, 6D** and quantified as the fold change w.r.t β -actin (**Figure.6E**). PLD2 expression is elevated in the lung tissues of mice challenged with bleomycin. This lung tissue lysates are inclusive of all the cell types present in the lung. This revealed that PLD2 may have important role to play in pulmonary fibrosis.

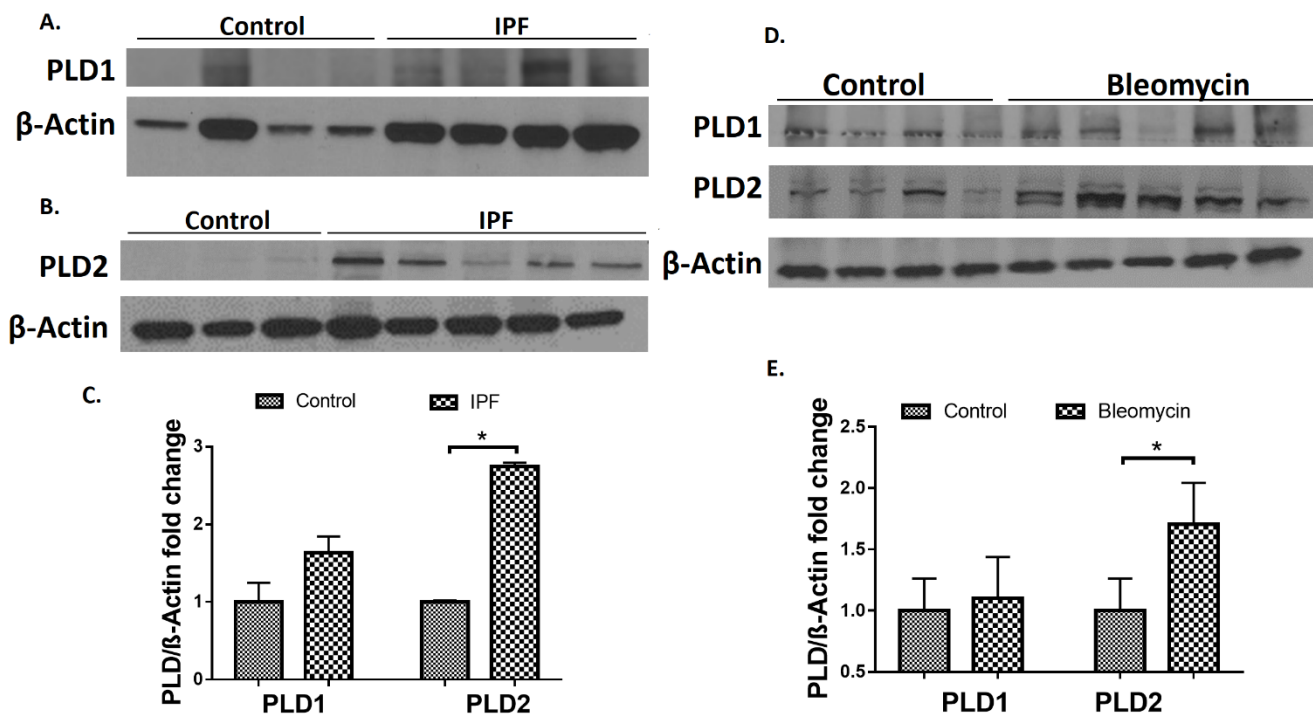


Figure 6: PLD2, but not PLD1 is up-regulated in lung tissues obtained from patients with IPF and bleomycin-challenged mice. Protein expression of PLD1 (A) and PLD2 (B) in lung homogenates from patients with IPF and donor control subjects as determined by Western blotting. C) Band intensities of PLD1 and PLD2 were quantified and normalized with β -Actin using ImageJ software. (D) C57BL/6 mice (6-8 weeks, male and female; n=4) were challenged with sterile PBS or bleomycin (1.5 U/kg in mouse) intratracheally and lungs were harvested on Day 14 post-bleomycin challenge. Protein expression of PLD1 and PLD2 in whole-lung homogenates was determined by western blotting. E.) Band intensities of PLD1 and PLD2 were quantified and normalized with β -Actin using ImageJ software. * $p < 0.05$

3.2 PLD expression in different cell types in IPF lung tissues:

PLD2 expression was found to be elevated in whole lung tissue lysates in IPF patients, which encompasses epithelial cells, endothelial cells, fibroblasts, among other cell types in the lung. To identify if the increased PLD2 expression is predominant in epithelial cells of the lung, epithelium being the first line of injury

during any insult to the lung; the paraffin embedded sections from normal and IPF patients were subjected to immunohistochemical staining for PLD2 and a cytokeratin marker to stain for epithelial cells in the lung. Increased PLD2 expression in IPF lung tissue sections was observed as compared to normal lung sections (**Figure.7**). Interestingly, PLD2 expression was not just increased in epithelial cells of the fibrotic lung, but also in other cell types present in the fibrotic foci.

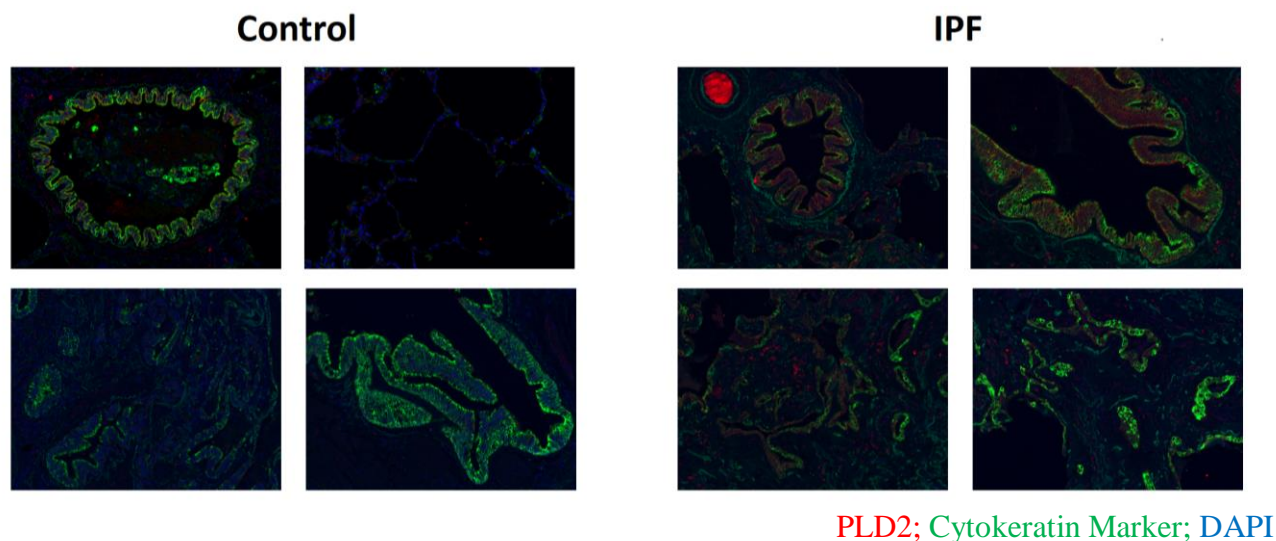


Figure 7: PLD2 staining in IPF lung tissue sections: Immunohistochemical staining was performed to determine the expression and localization of PLD2 in lung tissues from control subject and patients with IPF. Red regions indicate increased PLD2 expression in IPF specimens compared to control subjects.

3.3 Genetic deletion of *Pld2* in mice attenuates bleomycin induced lung injury and inflammation:

The role of PLD2 in bleomycin mediated inflammation in mouse lung was studied by whole body genetic deletion of PLD2 in mice. *Pld2*^{-/-} mice were viable and had similar phenotype to that of wild type mice as reported [56] (data not shown). Western blot analysis of the lung tissues showed that PLD2 expression in *Pld2*^{-/-} mice was almost knocked down (> 90%), without affecting PLD1 expression (**Figure. 8A**).

In bleomycin-induced PF, there is an initial inflammatory cascade in the mice lung that peaks at day 7 upon single-instillation of bleomycin to the mouse[57]. To validate the role of PLD2 in bleomycin-induced pulmonary fibrosis, wild-type and *Pld2*^{-/-} mice were challenged intratracheally with bleomycin (1.5 U/kg body weight) or sterile physiological saline and were evaluated for lung inflammation on day 7 post challenge. Bleomycin challenge of wild-type mice significantly increased lung damage as evaluated by H&E staining (**Figure. 8 B &C**), pulmonary leak as determined by elevated protein in bronchoalveolar lavage (BAL) fluid (**Figure.8 D**), infiltration of pro-inflammatory cells such as neutrophils and macrophages (**Figure. 8 E & F**) and IL-6 and TGF- β (Fig. 8G), which were attenuated in *Pld2* knockout mice challenged with bleomycin (**Figure. 8B-G**).

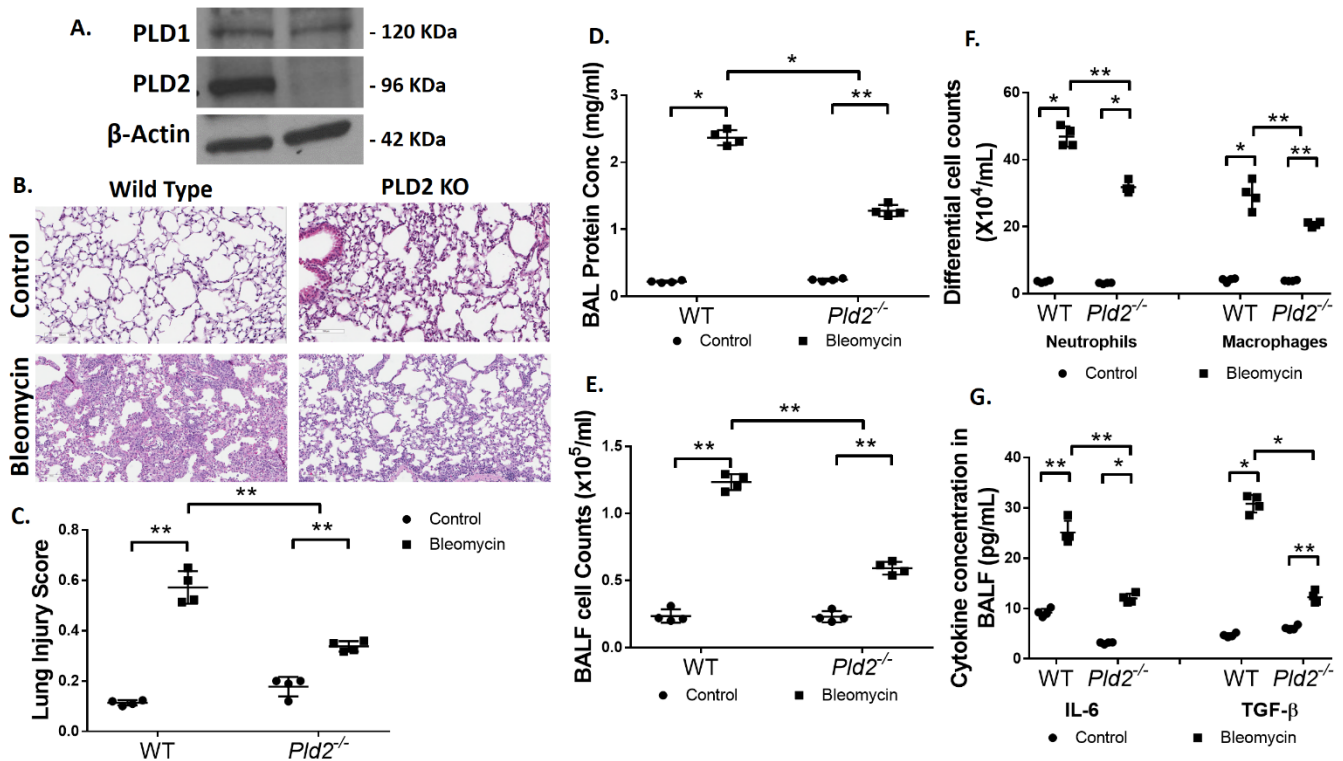


Figure 8: Genetic deletion of *Pld2* protects mice against bleomycin induced lung injury and inflammation. Male and female C57BL/6 Wild Type (WT) and *Pld2*^{-/-} mice (n=4 per group) were challenged intratracheally with bleomycin (1.5 U/kg in 50 μ l PBS) or sterile PBS and were sacrificed on Day 7 post bleomycin administration. Lungs were lavaged with sterile PBS solution, and the bronchoalveolar lavage (BAL) fluids were collected and analyzed as described in METHODS. Lung tissue sections were fixed in formalin and stained with hematoxylin and eosin (H&E) staining. (A) A representative Western blot showing PLD1 and PLD2 expression in WT and *Pld2*^{-/-} mice. (B) Representative H&E photomicrographs of lung sections obtained from WT and *Pld2*^{-/-} mice, scale bar = 100 μ m. (C) Acute lung injury score for each group. BAL fluids were analyzed for (D) total protein concentration, (E) total cell counts, (F) differential cell counts, and IL-6 and TGF- β levels. * $p < 0.05$, and ** $p < 0.005$

3.4 *Pld2*^{-/-} mice are protected from bleomycin induced pulmonary fibrosis:

In bleomycin-induced PF, after the initial inflammatory cascade, there is onset of fibrosis from Day 10 and by Day 21, there is extensive fibrosis followed by reversal after day 28 post-bleomycin challenge [58]. To assess the role of PLD2 in bleomycin-induced fibrosis, wild type and *Pld2*^{-/-} mice were treated with bleomycin, and lung tissues were harvested on day 21 and 28 post-bleomycin challenge. The BAL fluid was collected from the mice and the left lung was harvested for histology and right lung was harvested for other analysis. On Day 21, the bleomycin-induced significant lung tissue scarring in of wild type mice, whereas the lung tissues from *Pld2*^{-/-} mice were trending towards normal lung architecture, as seen from the Trichrome staining (**Figure.9A**) and quantified by the Ashcroft score (**Figure. 9B**). Furthermore, bleomycin- mediated soluble collagen levels, as measured by Sircol assay, were reduced in mice *Pld2*^{-/-} mice compared to wild type mice (**Figure. 9C**). The expression of fibrogenic proteins like fibronectin (FN) and collagen in the whole lung tissue lysates after bleomycin administration was significantly reduced in *Pld2*^{-/-} mice than wild type mice (**Figure. 9 D**). Bleomycin-induced apoptosis in the lung, as determined by TUNEL+ cells in the lung tissue sections after TUNEL staining, was significantly reduced in *Pld2*^{-/-} mouse lung as compared to wild-type (**Figure. 9 E&F**).

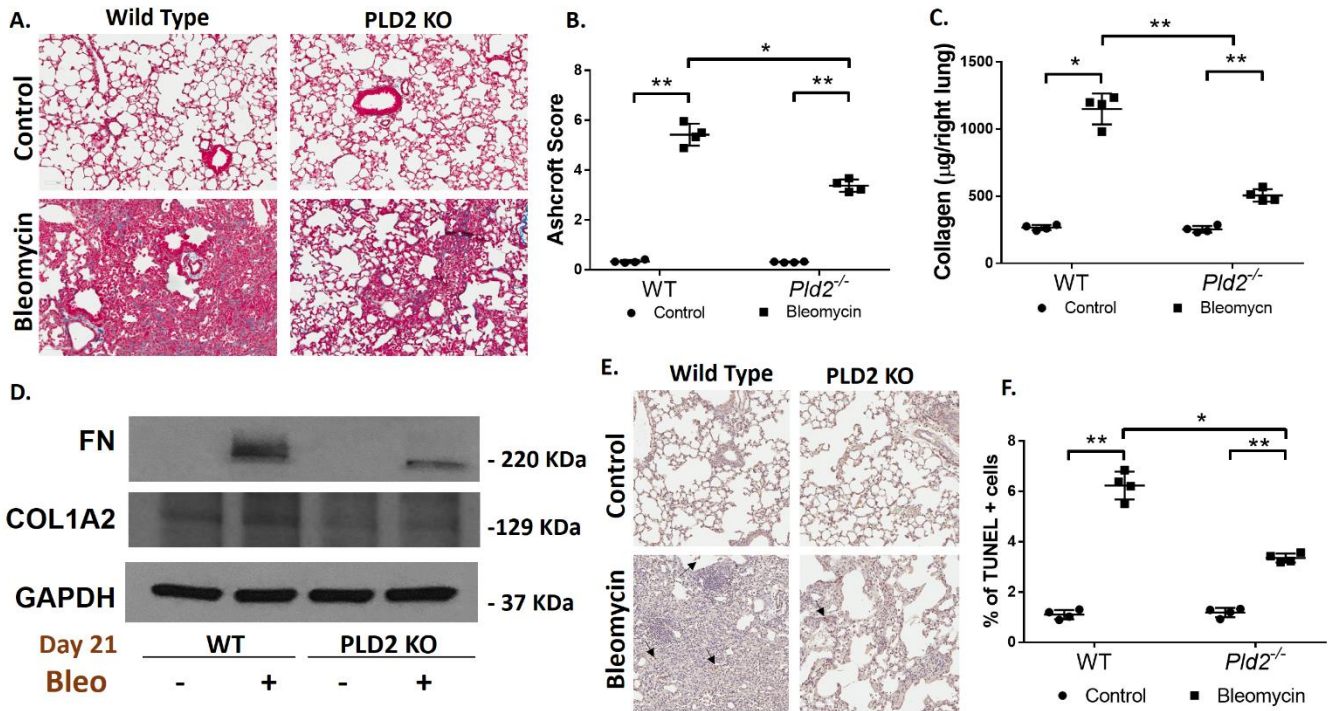


Figure 9: Genetic deletion of *Pld2* protects against bleomycin induced lung fibrosis in mice. Wild Type (WT) and *Pld2*^{-/-} mice were challenged intratracheally with bleomycin (1.5 U/kg in 50μl PBS) or sterile PBS and were sacrificed on Day 21 post bleomycin administration. **(A)** Representative photomicrographs of Masson's Trichrome staining of lung tissue sections from WT and *Pld2*^{-/-} mice with or without bleomycin challenge; the blue color indicating the collagen deposition. Scale bar = 100 μm. **(B)** Ashcroft score of lung sections. **(C)** Acid soluble collagen level in the lung tissue determined by Sircol Assay. **(D)** A representative Western blot showing protein expression of fibrotic markers, fibronectin and COL1A2 in the lung tissue with and without bleomycin challenge on day 21. **(E)** Representative photomicrographs of TUNEL staining of the lung tissue sections. Apoptotic nuclei are stained brown and marked by arrows. **(F)** The number of TUNEL-positive cells per field in the lung sections. * $p < 0.05$, and ** $p < 0.005$.

3.5 Genetic deletion of *Pld1* (*Pld1*^{-/-}) attenuates bleomycin-induced lung inflammation in mice:

Although PLD1 expression was not altered in lungs of IPF patients and bleomycin challenged mice (**Figure 6**), bleomycin has been shown to enhance total PLD activity in endothelial cells [44]. Therefore, in addition to PLD2, we also investigated the effect of genetic deletion of PLD1 in bleomycin-induced lung inflammation and pulmonary fibrosis in mice.

The role of PLD1 in bleomycin mediated inflammation in mouse lung was studied by whole body genetic deletion of PLD1 in mice. *Pld1*^{-/-} mice were viable and had similar phenotype to that of wild type mice as reported [59]. (data not shown). To validate the role of PLD1 in bleomycin-induced pulmonary fibrosis, wild-type and *Pld1*^{-/-} mice were challenged intratracheally with bleomycin (1.5 U/kg body weight) or sterile physiological saline and were evaluated for lung inflammation on day 7 post challenge. Bleomycin challenge of wild-type mice significantly increased lung damage as evaluated by H&E staining (**Figure 10 A & B**), pulmonary leak as determined by elevated protein in bronchoalveolar lavage (BAL) fluid (**Figure 10 C**), infiltration of pro-inflammatory cells such as neutrophils and macrophages (**Figure 10 D & E**) and IL-6 and TGF- β (**Figure 10 F**), which were attenuated in *Pld2* knockout mice challenged with bleomycin (**Figure 10 A-F**).

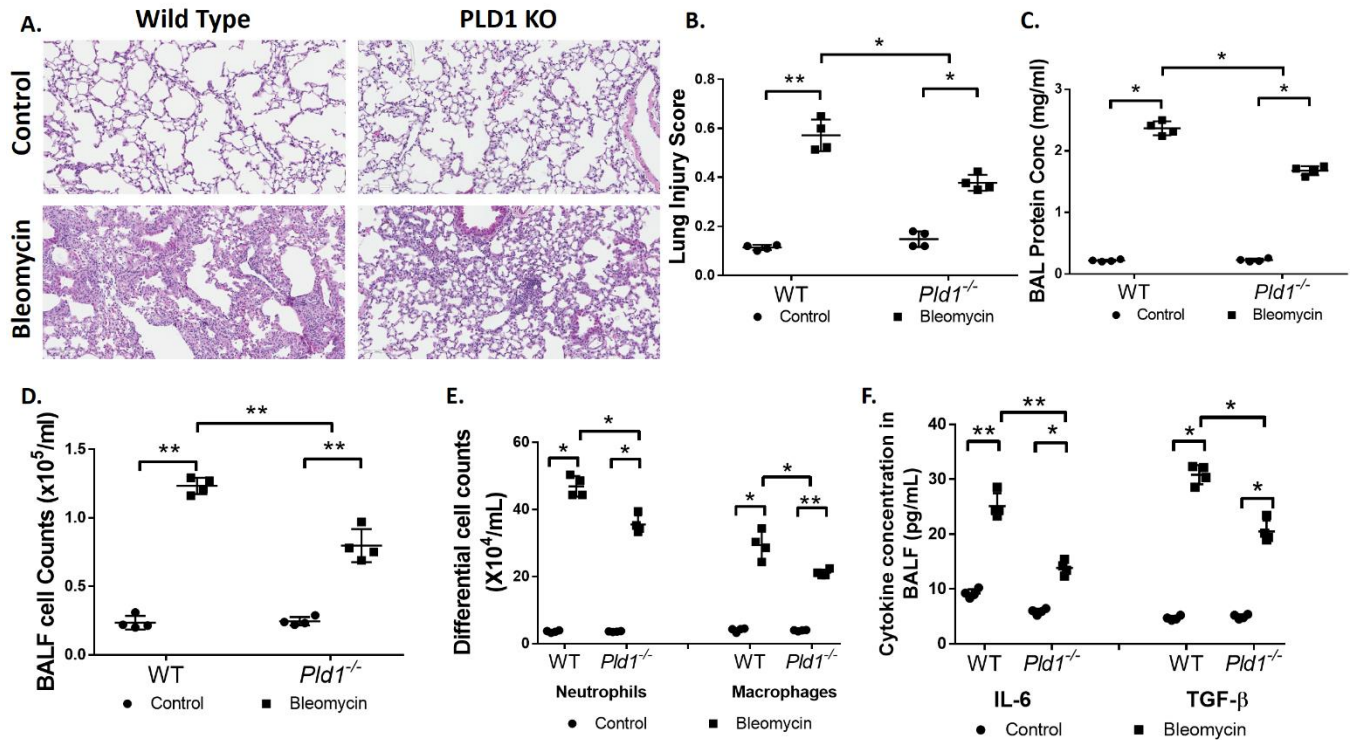


Figure 10: Genetic deletion of PLD1 protects against bleomycin induced lung injury and inflammation: Wild Type (WT) and *Pld1*^{-/-} mice were challenged with bleomycin (1.5 U/kg in 50 ml of PBS intratracheally, and were sacrificed on Day 7 post-administration. Lungs were lavaged with sterile PBS solution, and the bronchoalveolar lavage (BAL) fluids were analyzed as described in METHODS, and lung tissue sections were fixed in formalin and stained with hematoxylin and eosin (H&E) staining. (A) Representative H&E photomicrographs of lung sections obtained from WT and *Pld2*^{-/-} mice, scale bar = 100 μ m. (B.) Acute lung injury score in each group. BAL fluids were analyzed for (C.) total protein concentration, (D) total cell counts (E) differential cell counts (F.) IL-6 and TGF- β secretion. * $p < 0.05$, and ** $p < 0.005$ n=4 mice per group.

3.6 Genetic deletion of *Pld1* (*Pld1*^{-/-}) attenuates bleomycin-induced lung fibrosis in mice:

To assess the role of PLD2 in bleomycin-induced fibrosis, wild type and *Pld1*^{-/-} mice were treated with bleomycin, and lung tissues were harvested on day 21 post-bleomycin challenge. The BAL fluid was collected from the mice and the left lung was harvested for histology and right lung was harvested for other analysis. On Day 21, the bleomycin-induced significant lung tissue scarring in of wild type mice, whereas the lung tissues from *Pld1*^{-/-} mice were trending towards normal lung architecture, as seen from the Trichrome staining (**Figure 11A**) and quantified by the Ashcroft score (**Figure 11B**). Furthermore, bleomycin- mediated soluble collagen levels, as measured by Sircol assay, were reduced in mice *Pld1*^{-/-} mice compared to wild type mice (**Figure 11 C**). Bleomycin-induced apoptosis in the lung, as determined by TUNEL+ cells in the lung tissue sections after TUNEL staining, was significantly reduced in *Pld2*^{-/-} mouse lung as compared to wild-type (**Figure 11 D & E**).

Genetic knockdown of *Pld1* (*Pld1*^{-/-}) also attenuated bleomycin-induced lung inflammation and pulmonary fibrosis as compared to wild-type mice challenged with bleomycin; however, the protection was much lower compared to *Pld2* knock down in mice. These results suggest that genetic deletion of *Pld1* or *Pld2* confers protection against bleomycin-mediated lung fibrosis and PLD1 could compensate for PLD2 or vice versa in the knock out mice, which affects the development and progression of bleomycin-induced lung inflammation and PF in mouse lung.

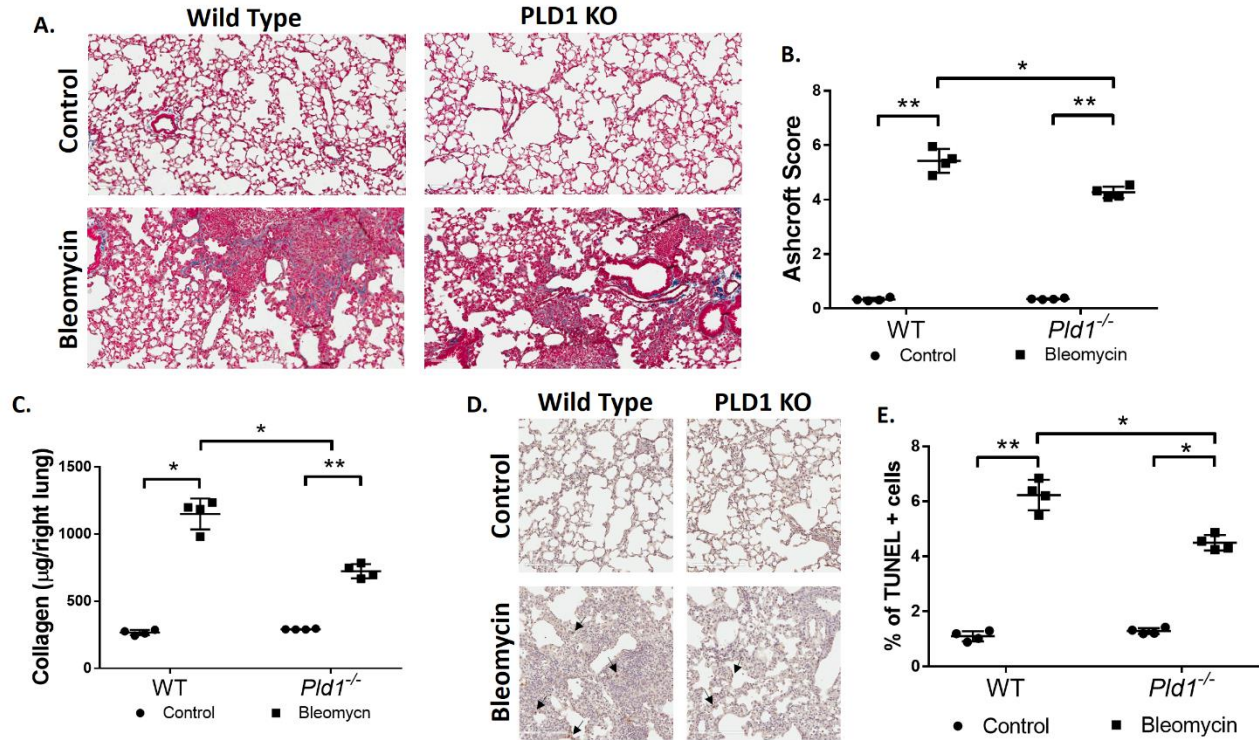


Figure 11: Genetic deletion of PLD1 protects against bleomycin induced fibrosis in mice: Wild Type (WT) and *Pld1*^{-/-} mice were challenged with bleomycin (1.5 U/kg in 50 ml of PBS intratracheally, and were sacrificed on Day 21 post administration. **A.** Representative photomicrographs of Masson's Trichrome staining of lung tissue sections from WT and *Pld1*^{-/-} mice, the blue color indicating the collagen deposition. Scale bar = 100 µm. **B.** Ashcroft score **C.** Acid soluble collagen level in the lung tissue determined by Sircol Assay **D.** Representative photomicrographs of TUNEL staining of the lung tissue sections. Apoptotic nuclei are stained brown and marked by arrows. **E.** The number of TUNEL-positive cells per high-power field in the lung sections. * $p < 0.05$, ** $p < 0.005$

3.7 Bleomycin enhances PLD expression and activity in epithelial cells and increases mitochondrial ROS:

In IPF lung specimens and lung tissues from bleomycin-challenged mice, immunohistochemistry revealed enhanced PLD2 expression in fibrotic foci as well as in endothelial and epithelial cells (data not shown). As lung epithelial cells play an important role in fibrogenesis, we sought to investigate *in vitro* the mechanism(s) by which PLD regulates bleomycin-induced lung inflammation and pulmonary fibrosis.

Total PLD activity and expression of PLD2, but not PLD1, was increased human bronchial epithelial cell line, Beas2B challenged with bleomycin for 24 h (**Figure 12 A-C**). These results show enhanced PLD activity and PLD2 expression in primary epithelial cells and an epithelial cell line, which could be used for studies related to mechanism(s) on regulation of fibrogenesis by PLD. At initial hours of bleomycin challenge, it was found to induce mitochondrial superoxide generation, as was seen by the enhanced fluorescence intensity of Mito SOX. (**Figure 12 D, E**).

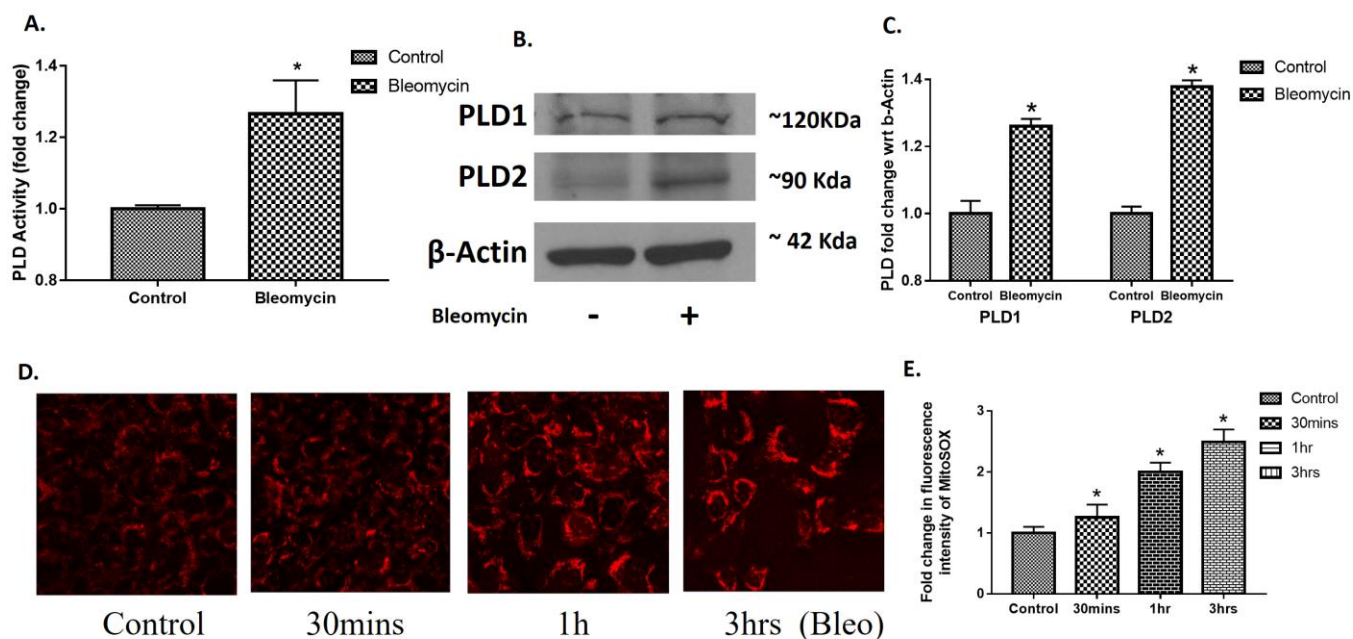


Figure 12: Bleomycin enhances PLD activity, PLD2 protein expression and mitochondrial ROS generation in Beas2B cells. Beas2B cells were challenged with 10mU bleomycin for 24 hrs. **A.** PLD activity was measured by Amplex™ Red assay kit. **(B).** Representative Western blot of PLD1, PLD2 and β -actin in total cell lysates from three independent experiments in triplicate. **(C)**, Quantification of the Western blots based by densitometry and fold changes were normalized to β -actin. Further, Beas2B cells were challenged with 10mU bleomycin for different time-points * $p < 0.05$, ** $p < 0.005$. **D.**

Representative images of Mito SOX staining from three independent experiments. E.) quantification of the fluorescence intensity of Mito SOX.

3.8 PLD regulates bleomycin-induced mitochondrial superoxide generation and modulation of oxidative stress in lung epithelial cells:

Recent studies suggest a role for mitochondrial- and NOX-dependent ROS generation in promoting pulmonary fibrosis in IPF and bleomycin murine model of lung fibrosis [60]. Also, we and others have demonstrated a role for PLD mediated generation of phosphatidic acid (PA) signaling in hyperoxia- or phagocyte-induced ROS generation [61]. Bleomycin challenge results in alveolar epithelial injury leading to activation and proliferation of myofibroblasts[62]; therefore we investigated the role of PLD in bleomycin-mediated mitochondrial superoxide production and regulation of antioxidant enzymes like MnSOD in lung epithelial cells. MnSOD acetylation indicates inactivation of the enzyme, thus leading to impaired oxidative stress induced repair[63].

Challenge of Beas2B cells with bleomycin enhanced mitochondrial superoxide production as quantified by Mito SOX staining, which was blocked by pretreatment of cells with specific PLD1 inhibitor, VU0155069 (250 nM) or PLD2 inhibitor, VU0364739 (500nM) (**Figure 13A & B**). As blocking PLD1 or PLD2 separately reduced bleomycin-induced mitochondrial ROS generation by ~30% compared to cells with no inhibitor, cells were pre-incubated with both PLD1 and PLD2 inhibitors to determine the mitochondrial superoxide production. Pretreatment with PLD1 and PLD2 inhibitors together reduced the mitochondrial ROS generation by bleomycin ~60% as compared to control cells (**Figure 13B**). Further, it was also observed that there was increased acetylation of MnSOD^{K68} in Beas2B cells challenged with bleomycin which was reverted by PLD2 inhibition, as determined by western blotting (**Figure 13 C**),

and quantified (**Figure 13 D**). These results suggest that PLD1 and PLD2 are involved in bleomycin-induced mitochondrial superoxide generation and modulation of the antioxidant enzymes in Beas2B cells.

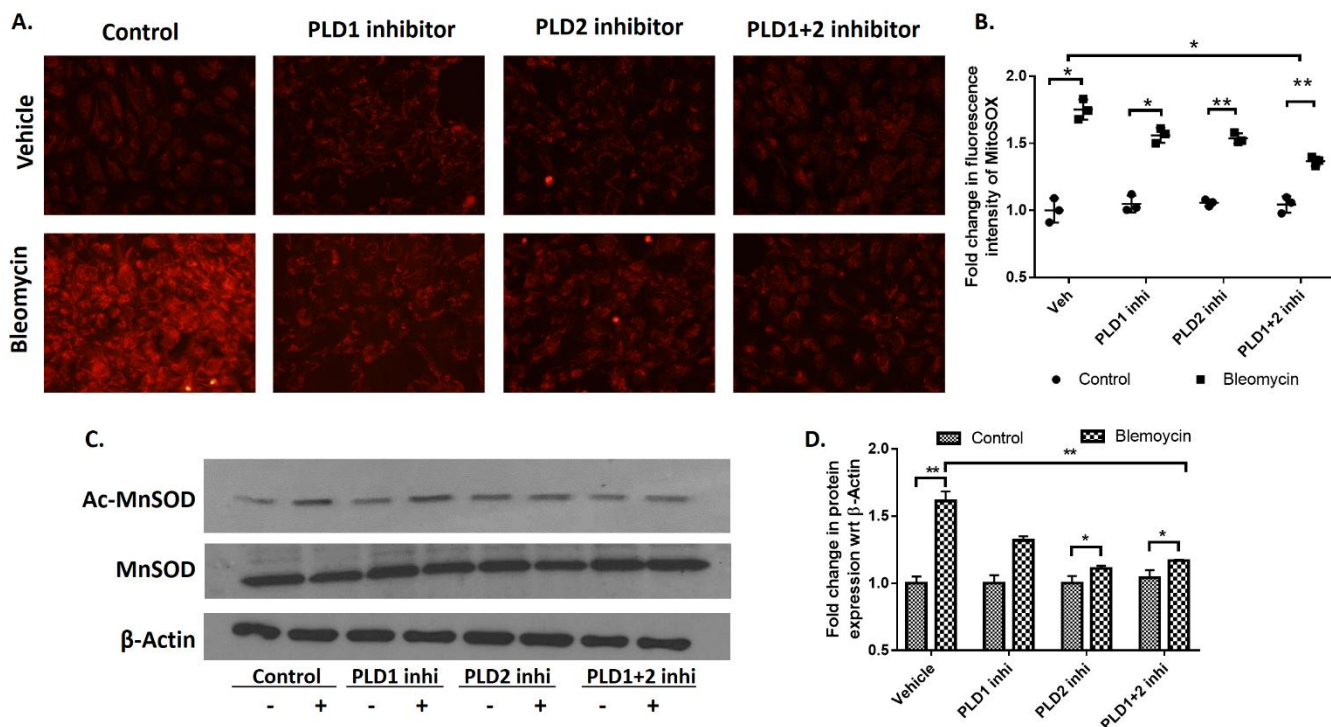


Figure 13: Inhibition of PLD1 and PLD2 activity attenuates bleomycin-induced mitochondrial ROS generation and modulation: Beas2B cells grown in 35-mm dishes (~90% confluence) were pre-treated with 250nM PLD1 inhibitor (VU0155609), 500nM PLD2 inhibitor (VU 0364739) or 250 nM VU0155609 + 500 nM VU0364739 for 3h prior to bleomycin challenge (10mU/ml) for 1 hr. Cells were then incubated with Mito SOX™ red reagent for 15 min and later subjected to two washes with phenol red free media. (A) Representative images of MitoSOX staining, a measure of mitochondrial superoxide generated. (B) Quantification of the fluorescence intensity of MitoSOX by Image J. In separate experiments, the cells lysates were harvested and analyzed by Western blotting for MnSOD acetylation at K68. (C.) Bleomycin was found to enhance acetylation of MnSOD⁶⁸ in Beas2B cells which was found to be attenuated by blocking PLD. (D.) Quantification of the Western blots by densitometry/Image J

analysis and fold changes were normalized to total MnSOD and β -actin. Values are means \pm SD of three independent experiments. * $p < 0.05$, ** $p < 0.005$

3.9 Inhibition of PLD attenuates bleomycin-induced mitochondrial DNA damage in lung epithelial cells:

Recent evidence implicates uncontrolled generation of mitochondrial superoxide by agents such as bleomycin and asbestos induces mitochondrial DNA damage and pulmonary fibrosis [48, 64]. Having demonstrated a role for PLD in bleomycin-induced mitochondrial superoxide generation, next we assessed whether PLD regulates mitochondrial DNA damage using a Q-PCR based assay, which determines both nuclear and mitochondrial DNA [55]. Treatment of Beas2B cells with mito TEMPO (100 μ M), a scavenger of mitochondrial ROS, decreased mitochondrial superoxide and mitochondrial DNA damage (**Figure 14 A**). Pretreatment of Beas2B cells with VU0155069 (PLD1-selective) or VU0364739 (PLD2-selective) reduced bleomycin-induced mitochondrial DNA damage by almost four-fold (**Figure 14B**). Simultaneous addition of PLD1 and PLD2 inhibitors to cells did not further reduce bleomycin-induced mitochondrial DNA damage (**Figure 14 B**). Collectively, these data show that activation of PLD leads to mitochondrial ROS mediated mitochondria DNA damage in lung epithelial cells.

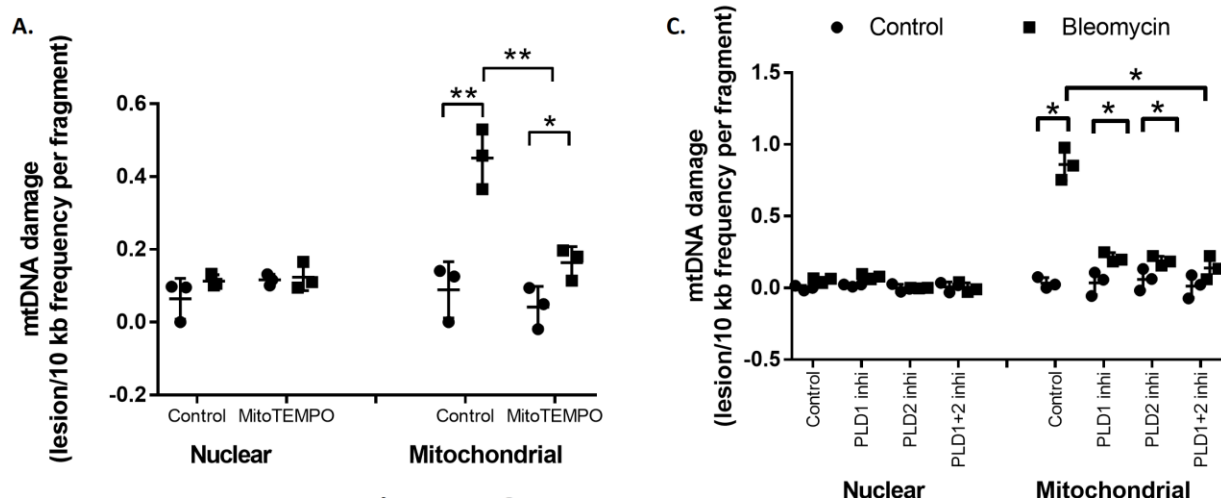


Figure 14: Inhibition of mitochondrial superoxide generation and PLD attenuates bleomycin-induced mtDNA damage in bronchial epithelial cells: (A) Beas2B cells grown in 35-mm dishes (~90% confluence) were treated with Mito Tempo (100 μ M) for 3 h prior to exposure to bleomycin (10 mU/ml) for 24 h. (B) Beas2B cells in 35-mm dishes (~90% confluence) were pre-treated with 250nM PLD1 inhibitor (VU0155609), 500nM PLD2 inhibitor (VU 0364739) or a mixture of 250 nM PLD1 and 500 nM PLD2 inhibitors for 3 h prior bleomycin challenge (10mU/ml) for 24 h. MtDNA damage was determined by qPCR-based measurement using isolated whole genomic DNA-both mitochondrial and nuclear DNA as indicated in Methods. DNA damage was expressed as the ratio of lesion frequency per fragment. Values are means \pm SD from three independent experiments in triplicate. * $p < 0.05$, ** $p < 0.005$

3.10 Inhibition of PLD attenuates bleomycin-induced epithelial cell apoptosis:

There is compelling evidence implicating that oxidative-stress mediated mitochondrial DNA damage promotes epithelial cell apoptosis and pulmonary fibrosis [48]. Having shown a role for PLD in bleomycin-induced mitochondrial DNA damage via mitochondrial ROS, we next studied the effect of PLD inhibition on bleomycin-induced epithelial apoptosis. Blocking mitochondrial ROS using 100 μ M mitoTEMPO reduced bleomycin-induced apoptosis in Beas2B cells (**Figure 15A-D**) as determined by cleaved PARP and Caspase 3 and flow cytometry of Annexin V and PI positive cells. Further, inhibition of both PLD1 and PLD2 simultaneously was more effective in attenuating bleomycin-induced apoptosis

(Figure 15 E-J). These results support an important role for PLD in oxidative stress mediated bleomycin induced epithelial cell apoptosis.

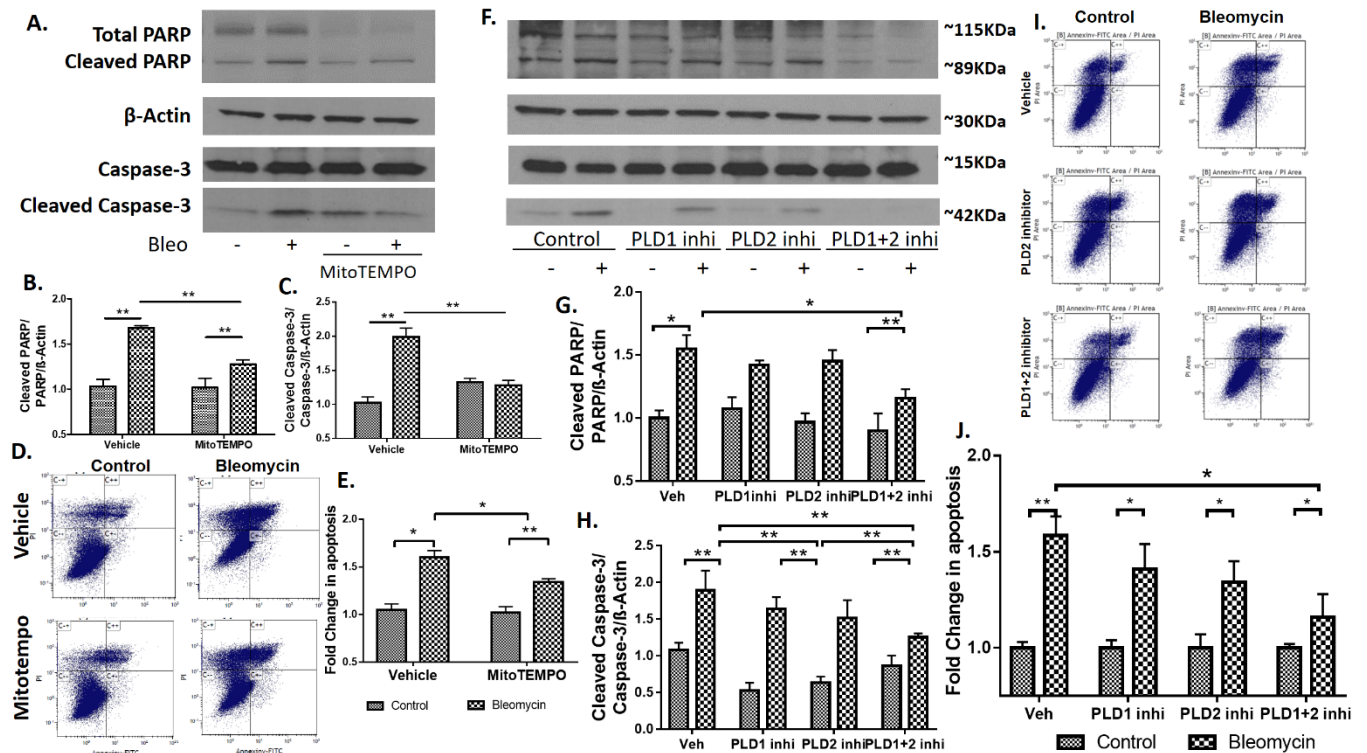


Figure 15: Inhibition of mitochondrial superoxide generation and PLD activity attenuates bleomycin induced apoptosis in bronchial epithelial cells: Beas2B cells grown in 35-mm dishes (~90% confluence) were treated with Mito Tempo (100 μM), 250nM PLD1 inhibitor (VU0155609), 500nM PLD2 inhibitor (VU 0364739), or a combination of 250 nM PLD1 and 500 nM PLD2 inhibitors for 3 h prior bleomycin challenge (10mU/ml) for 24 h. Programmed cell death following bleomycin challenge was determined by cleavage of Caspase-3 & PARP, indicators for apoptosis and flow cytometry of Propidium iodide/annexin V positive cells. (A) Protein expression of Caspase-3 and PARP in the cell lysates from cells with or without Mito tempo after Western blotting. (B & C) Quantification of cleaved Caspase-3 and PARP from (A) by densitometry and Image J analysis and data were normalized to β-Actin levels. (D & E) Beas2B cells were exposed to bleomycin in the absence or presence of Mito Tempo as in (A) and apoptosis was quantified by flow cytometry analysis, which can sort early apoptotic and late apoptotic cells by labelling the cells with Annexin V and Propidium iodide (PI). (F-H) Cell lysates from control and PLD1, PLD2

and PLD1 + PLD2 inhibitor treated cells with and without bleomycin challenge were analyzed by Western blotting for cleaved PARP and Caspase-3 and total β -actin. The band intensities were quantified by densitometry and Image J. Shown is a representative blot from three independent experiments. (I & J) Cells pre-treated with PLD1, PLD2 or PLD1 +PLD2 inhibitors in the presence or absence of bleomycin (10mU/ml) for 24 h were analyzed by flow cytometry. Shown is a representative dot plots of annexin V and PI staining. The Annexin V+/PI+ were the late apoptotic cells as seen in C++ quadrant, and Annexin V+/PI- cells were early apoptotic cells as seen in C+-. (J) the percentage of late apoptotic cells were quantified. * $p < 0.05$, ** $p < 0.005$

4. DISCUSSION

Idiopathic pulmonary fibrosis is a progressive disease of unknown etiology leading to mortality, due to lack of effective therapeutic strategies. One of the most important mechanisms in IPF is repeated injury to the lung epithelium that leads to its dysfunction through dysregulated wound repair. Abnormal bronchiolar and hyperplastic type II epithelial cells that line the honeycomb regions are distinctly present in IPF tissues in addition to fibroblastic foci containing fibroblasts and myofibroblasts[65]. The lung epithelium being the first line of injury during any insult to the lung; elucidating the altered signaling mechanism in the lung epithelium is necessary to identify therapeutic strategies for the disease. Here, we provide *in vivo* evidence demonstrating that genetic knocking down of *Pld2* in mice rendered protection against bleomycin-induced lung injury and inflammation, as seen by the histological changes in the lung on day 7 after bleomycin instillation, cytokine analysis, and infiltration of cells into the bronchoalveolar lavage fluid (**Figure 8**). Further, bleomycin induced fibrosis in the lung was attenuated in *Pld2*^{-/-} mice, as seen in the reduction in collagen deposition in the lung and the expression of fibronectin on day 21 (**Figure 9**). Also, the recovery from bleomycin induced fibrosis as seen on Day 28 upon bleomycin instillation was enhanced in *Pld2*^{-/-} mice than in wild type mice (data not shown). *Pld2*^{-/-} mice were only partially protected against bleomycin-induced PF, which might be due to the compensatory role of PLD1. We also found that knockdown of *Pld1* in mice also offered some protection against bleomycin induced PF, though not comparable to *Pld2* deficient mice. These results established that genetic ablation of *Pld1* or *Pld2* ameliorated bleomycin induced PF. Further, we demonstrated for the first time that down-regulation of PLD2 or inhibition of PLD2 activity attenuated bleomycin-induced mitochondrial DNA damage and apoptosis of alveolar epithelial cells suggesting that PLD2 may be a potential therapeutic target against lung fibrosis.

Of the six PLD isoforms, PLD1-6, only PLD1 and PLD2 exhibit catalytic activity [21], and hydrolyze phosphatidylcholine (PC) to phosphatidic acid (PA) and choline[41]. In addition to PC, PLD1 and PLD2 can also use other phospholipid such as phosphatidylethanolamine, and phosphatidylserine as phospholipid substrates and mitochondrial PLD6 utilizes cardiolipin to generate PA. In the present study, lung tissues from IPF patients and bleomycin induced murine model of fibrosis showed enhanced PLD2 expression compared to PLD1; however, PLD1, but not PLD2, expression was increased in DMN-induced rat liver fibrosis [42]. Further, blocking PLD activity with N-methylethanolamine (MEA) reduced rat liver fibrosis by DMN by modulating TIMP1 and collagen 1A1 expression[42] with no change in TGF- β and MCP1 expression. Genetic deletion of *Pld2* or inhibition of PLD2 with a specific inhibitor reduced bleomycin-induced FN and COL1A1 expression suggesting a role for PLD2 activity in regulating bleomycin mediated fibrogenic and extracellular matrix proteins. In contrast to requirement of PLD1 or PLD2 activity in the development of liver or lung fibrosis, respectively, mice subjected to either folic acid (FA) or surgical unilateral ureteral obstruction (UUO) developed kidney fibrosis, which was dependent on expression of PLD4 [32]. PLD4 is a transmembrane glycoprotein, has no enzyme activity, and unlike PLD1 and PLD2, lacks Phox (PX) and pleckstrin homology (PH) domains in the N-terminal region and two conserved His-x-Lys-x-x-x-x-Asp sequence (x is HKD) motifs in the C-terminus region. Global or proximal tubule epithelial cell specific PLD4 knockdown conferred protection against FA- or UUO-induced kidney fibrosis in mice [32]. While the mechanism of PLD4 in the development of FA- or UUO-induced kidney fibrosis is unclear, PLD4 was found to interact with neutral elastase, and neurotropic receptor tyrosine kinase (TrkA) 1 to modulate mitogen-activated protein kinase in proximal tubule epithelial cells [32]. PA generated through PLD pathway is an important second messenger and has been implicated in cell migration [66], proliferation [67], cytoskeletal reorganization [68], NADPH oxidase activation [69], and vesicular trafficking[70]. Further, PLD derived PA serves as a precursor for

diacylglycerol (DAG) and lysophosphatidic acid (LPA), which are bioactive lipid mediators involved in cell signaling and function. Lipid phosphate phosphatases hydrolyze PA to DAG [71], which activates classical and atypical PKC isoforms including PKC α , β and δ in mammalian cells. TGF- β stimulated collagen synthesis was dependent on PKC δ activation in human lung fibroblast [72] while PKC β II and PKC δ - mediated inactivation of p38 MAPK signaling modulated cardiac fibroblast proliferation and collagen deposition [73]. However, in human lung fibroblasts, CCL18 stimulated collagen production was PKC α , but not PKC δ or PKC ϵ dependent [74]. The contradictory role of various PKC isoforms in collagen production in fibroblasts is unclear but may be related to different stimuli and types of fibroblasts used. LPA is another lipid second messenger that has been implicated in IPF and bleomycin-induced pulmonary fibrosis [75]. LPA is generated either from PA by the action of PA specific phospholipase A1 or A2 [76, 77] or from lyso PC by autotaxin (ATX) [78]. Genetic deletion of LPA1 and LPA2 in mice or inhibition of ATX protected mice from bleomycin-induced pulmonary fibrosis [75, 79, 80]. However, a recent study has demonstrated that ATX activity, although increased following bleomycin-induced lung injury, may not be required for pulmonary LPA production or fibrosis [81]. Further studies are necessary to determine the role of PLD1 and/or PLD2 in local generation of LPA and its role pulmonary fibrosis.

A novel finding of this study is the role of PLD2 in regulating bleomycin-induced mitochondrial ROS generation, which can lead to mitochondrial DNA damage and apoptosis in lung epithelial cells. Superoxide is an important oxidant that regulates the oxidative stress, apart from hydrogen peroxide, and hydroxyl radical [82]. Physiologically, low levels of ROS are generated in cells, which are essential for various cellular processes like gene expression, migration, proliferation and differentiation[83]. However, in case of excess ROS generation, as in the case of IPF, the redox equilibrium is disrupted and there is oxidative stress induced damage in the cells and tissues [84]. Enhanced generation of ROS resulting in oxidative stress has been implicated in bleomycin-induced pulmonary fibrosis[85] and IPF [86]. Oxidative

stress causes lung epithelial cell apoptosis, differentiation and proliferation of lung fibroblasts and modulation of TGF- β signaling through Smad pathway [87], which is central to fibrogenesis. Hydrogen peroxide derived from NADPH oxidase (Nox) 4 and superoxide from mitochondrial electron transport chain are two major source of ROS generated in bleomycin model of lung fibrosis and IPF [49, 85, 88]. Recent evidence shows that inhibition of TGF- β -induced mitochondrial ROS generation attenuates pro-fibrotic gene expression and targeting mitochondrial ROS might be a therapeutic approach in treating excessive fibrosis associated pathologies [87].

In lung epithelial cells, bleomycin stimulated mitochondrial ROS production that was attenuated by inhibition of PLD1 or PLD2 activity by specific inhibitors (**Figure 13A**). Interestingly, inhibition of both PLD1 and PLD2 simultaneously was more effective in reducing bleomycin-induced mitochondrial ROS generation as compared to the inhibitors alone suggesting compensatory role for PLD1 or PLD2 in generation of PA and signal transduction. The mechanism(s) of PA-mediated regulation of mitochondrial electron transport chain and superoxide generation is unclear. Cell surface receptors for PA have not been identified and PA generated intracellularly modulates signaling cascades via non-receptor mediated pathways. PA generated by the activation of PLD1 or PLD2 has been shown to activate PKC ζ [89], phosphatidylinositol 4-kinase [25, 90, 91], and sphingosine kinase 1 [92] in mammalian cells. More recently, a role for PLD/PA signaling axis in activation of IQGAP1 through Rac1 in hyperoxia-mediated ROS generation in lung ECs was demonstrated suggesting PA generated by the PLD pathway to be a potent activator of NADPH oxidase (Nox) proteins [45].

Interestingly, we observed that PA generated from PLD2 also regulates MnSOD activity in lung epithelial cells. Superoxide is one of the important oxidants that regulates the oxidative stress, apart from hydrogen peroxide (H₂O₂), and the hydroxyl radical [85]. Physiologically, lower levels of ROS are present and these are essential for various cellular processes like gene expression, migration, proliferation and

differentiation[93]. However, in case of excess ROS generation, as in the case of IPF, the redox equilibrium is disrupted and there is oxidative stress induced damage in the cells and tissues [84].

Superoxide dismutases (SOD) is one of the important antioxidant defense mechanisms in the lung [94], and specifically mitochondrial manganese SOD (MnSOD) plays an important role in maintaining mitochondrial redox status. This enzyme detoxifies superoxide by catalyzing its dismutation to H₂O₂. Bleomycin increases acetylation of manganese superoxide dismutase (MnSOD^{K68}) in Beas2B cells (**Figure 13C**), and acetylation of MnSOD has been shown to inactivate the enzyme, and enhance oxidative stress-induced damage to the lung [63]. Inhibition of PLD2 activity with PLD2 specific inhibitor, VU0364739, blocked bleomycin-induced acetylation of MnSOD^{K68}, whereas blocking PLD1 activity had no effect on acetylation of MnSOD (**Figure 13C**). Alveolar type II cells isolated from IPF lungs showed increased MnSOD K68 acetylation compared with controls due to decreased SIRT3 protein expression [50]. SIRT3 is a mitochondrial member of the sirtuin family of NAD-dependent deacetylases [95, 96], and blocking SIRT3 reduced oxidant-induced mitochondrial DNA damage and apoptosis [50]. The results presented here show a role for PLD/PA signaling in MnSOD acetylation and does not address the role of PLD1 or PLD2 in modulating SIRT3 expression or activity and fibrosis, and further studies are necessary.

Another important finding in this study is that inhibition of PLD1 or PLD2 ameliorated bleomycin-induced mitochondrial DNA damage (**Figure 14 B**) and apoptosis (**Figure 15 F-J**) in alveolar epithelial cells. The role of mitochondrial ROS in mitochondrial damage and apoptosis was verified by using a mitochondrial ROS specific scavenger, Mito Tempo. Mito Tempo pre-treatment of alveolar epithelial cells attenuated bleomycin-mediated mitochondrial ROS, mitochondrial damage and apoptosis (**Figure 14A, 15 A-E**). These findings confirm the earlier reports on increased mitochondrial superoxide production causing mitochondrial DNA damage and apoptosis of lung alveolar epithelial cells [48].

The near proximity of mtDNA to electron transport chain (ETC), inadequate DNA repair mechanism and its lack of histone protective shield to cover it makes it more susceptible to damage induced by oxidative stress than nuclear DNA, almost 50-fold more [97]. MtDNA damage leads to reduction in mitochondrial membrane potential and thereby alters the efficiency of ETC, thus contributing to the enhanced outer mitochondrial membrane permeability [98]. In addition, mtDNA damage is followed by release of proapoptotic agents like caspase-3, Bax, cytochrome c, Apaf-1 and downregulation of anti-apoptotic proteins like Bcl-2[99]. Concurrently results in our study also showed that blocking mitochondrial superoxide using mitoTEMPO blocked mitochondrial ROS generation. Further, blocking both the PLD isoforms was essential to block apoptosis.

4.2 Conclusion:

This study thus reveals the vital role of phospholipaseD2 in mediating pulmonary fibrosis (PF), thereby identifying PLD2 as a possible therapeutic target in IPF. Genetic deletion of PLD2 in mice was found to be protective against bleomycin induced fibrogenesis in mice. PLD2 was found to regulate lung fibrosis in by inducing oxidative stress, which further leads to mtDNA damage and thus promotes AEC apoptosis and pulmonary fibrosis. Thus, targeting PLD2 in the lung epithelium could be a viable therapeutic strategy against PF. Currently there are no studies showing the impact of inhibition of PLD2 in humans. There shouldn't be possible deleterious impact on the deletion of PLD2, owing to the compensatory effect of the other major PLD isoform, PLD1. The impact of blocking PLD in humans warrants further studies to confirm that there are no critical complications.

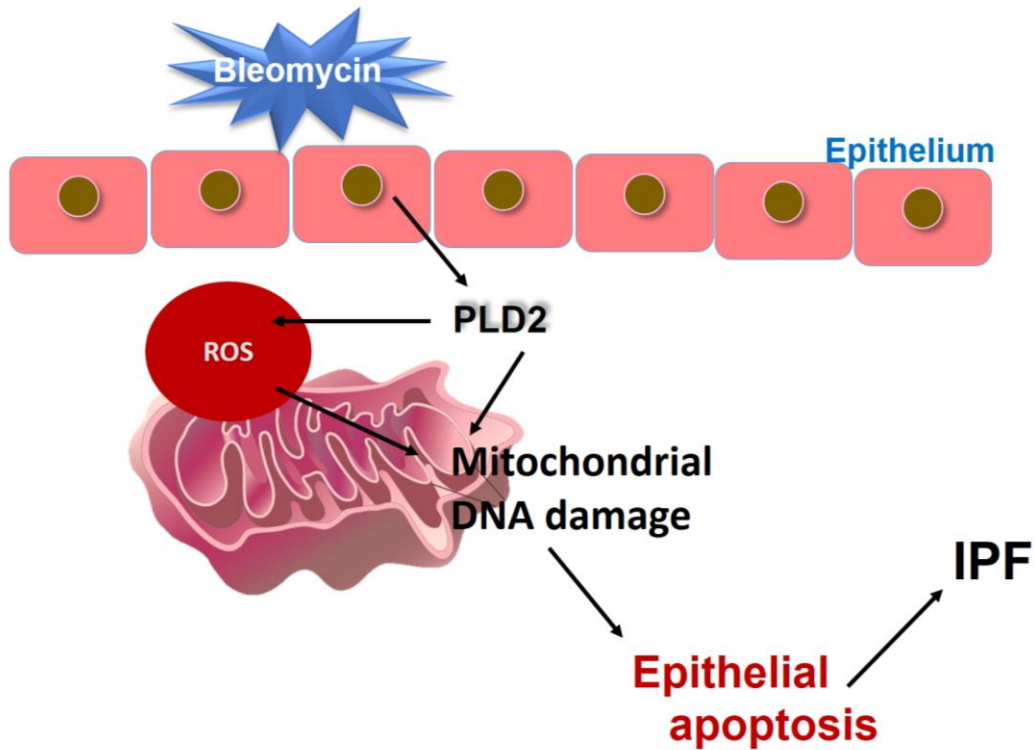


Figure 16: Proposed mechanism of PLD2 in bleomycin-induced activation of mitochondrial ROS, mitochondrial DNA damage and apoptosis of bronchial epithelial cells: Bleomycin challenge stimulates expression and activity of PLD2 in bronchial epithelial cells. Activated PLD2 generates phosphatidic acid and enhances mitochondrial superoxide production, which leads to mitochondrial DNA (mtDNA) damage and apoptosis of bronchial epithelial cells. These events result in increased expression of fibrogenic markers and development of lung fibrosis in bleomycin murine model of pulmonary fibrosis.

4.3 Future directions:

Having established a role for PLD1 and PLD2 in bleomycin induced pulmonary fibrosis and how PLD2 regulates mitochondrial damage mediated apoptosis in the epithelial cells, the effect of reversal of bleomycin induced epithelial injury and apoptosis on IPF would be evaluated by using preclinical models of fibrosis wherein PLD2 will be deleted in the epithelium. PLD2^{flox/flox} and PLD2^{Δae} mice will be used. (PLD2^{Δae} will be generated by breeding PLD2^{flox/flox} with SPC-Cre). Minimal or no fibrosis PLD2^{Δae} mice upon bleomycin challenge when compared to PLD2^{flox/flox} would establish the fact that deletion of PLD2 in epithelial cells in the mice would be a therapeutic strategy against IPF. In IPF lung specimens PLD2, in addition to the epithelial cells, was also expressed in other cell types (**Figure 7**); therefore, another approach will be to generate mice lacking both PLD1 and PLD2 as each of the isoforms compensate for the lack of the other, to a certain extent. Mice knockdown with PLD1 and PLD2 are viable and use of these mice in the bleomycin model will assert PLD targeting as a therapy in pulmonary fibrosis.

Chapter II: Fourier transform infrared imaging identifies biochemical changes in pulmonary fibrosis in a label-free manner

5. INTRODUCTION

The current diagnostic approaches for IPF are complex and suboptimal. The diagnosis requires both imaging and histologic evaluation, and therefore depends on a multidisciplinary discussion between a pulmonologist, radiologist, and pathologist [100]. High resolution computed tomography (HRCT) imaging offers the initial detection of IPF based on several radiological features [101], but the diagnosis must be validated in cases where the clinical and imaging information are insufficient to exclude other causes of interstitial lung disease.

This validation is accomplished by lung biopsy followed by histopathological analysis to demonstrate characteristic features and exclude alternative diagnoses [102, 103]. But this technique, which consists of chemical staining and labeling to enhance contrast in light microscopy is not only time consuming, but is also of limited statistical confidence due to manual interpretation and the potential for stains to perturb the function of small metabolites [104]. Label-free chemical imaging approaches, on the other hand, are emerging as a quantitative, automated means of assessing the chemical and morphological changes of tissue samples.

1.a Fourier transform infrared imaging (FT-IR):

FT-IR is one of these hyperspectral imaging techniques that assesses the chemical status of a tissue without the need for exogenous labels [105]. This method combines the morphological information gleaned from microscopy with a biochemical profile derived from the sample's infrared absorption spectrum, and offers a means to selectively analyze the chemical compositions of different features of diseased tissues[106]. In

recent years, FT-IR applications to histopathology have increasingly focused on diseases of connective tissue and on fibrotic processes in a variety of organ systems [107].

FT-IR imaging combines imaging at a spatial resolution that approaches light microscopy coupled with the biochemical sensitivity of spectroscopy. It is based on the principle that chemical bonds absorb different frequencies of mid-infrared light. Chemical bonds (such as C-H, N-H, O-H) form the basis of key cellular biomolecules such as proteins, lipids, collagen, glycogen, DNA and RNA, which allows for the acquisition of a “biochemical signature”, termed a spectrum, of the sample. In FT-IR imaging mode, a spectrum is acquired at every pixel within an image, therefore while visible images are typically comprised of only three channels; red, green and blue, in FT-IR each pixel is composed of hundreds of biochemical channels. These information-rich biochemical images can then be used towards cell type classification, disease diagnosis or understanding disease progression.

There are very significant technological and computational advances over the past few years have been of critical importance in making this technology amenable for the assessment of fibrosis: 1) huge increases in speed of data acquisition due to availability of large multi-element detectors allowing for imaging of tissue sections in minutes, 2) new instrument designs that permit up to 1x1 micron spatial resolution while retaining high-fidelity spectral data, and, 3) advanced computational tools that allow us to mine these data sets for classification.

This research presents FT-IR imaging of biochemical alterations occurring in lung fibrosis in preclinical models of IPF. A well-accepted murine model of bleomycin-induced pulmonary fibrosis was used [108], creating a disease course with rapid onset of alveolar damage (7 days) and progressive fibrosis (14 days to 21 days) with resolution within one month (28 days) [109]. FT-IR data from lung sections at weekly time points from induction to resolution were compared to conventional histopathological evaluation, and

investigated with ratiometric and multivariate analysis techniques to search for biochemical markers of disease onset and progression.

6. MATERIALS AND METHODS

6.1 Bleomycin induced PF in mice:

All animal experiments were carried in accordance with the procedures approved by the Institutional Animal Care and Use committee at the University of Illinois at Chicago, called the Animal Care Committee (Protocol # 15-240). The bleomycin-induced rodent model for pulmonary fibrosis was developed as per the review of various animal models of IPF by Moore et al[110]. Mice were anesthetized with a mixture of ketamine (100 mg/kg) and xylazine (5 mg/kg) for bleomycin instillation. The rodent was placed at 45° angle on a platform hanging by its incisors. The tongue was pulled out gently and held to the side using forceps, and 1.5 U/kg of body weight of bleomycin sulfate (Hospira Inc., Lake Forest, IL, USA) was given to the mouse by intratracheal injection with a maximum volume of 50 µL. The mouse was then taken out of the platform and placed under a heating lamp for a few minutes, before returning it to the cage.

Based on the time point of harvest post-bleomycin challenge, the animals (N=3 in each group) were grouped as 1. Control; 2. Day 7 (Inflammation); 3. Day 14 (Onset of fibrosis); 4. Day 21 (fibrosis); and 5. Day 28 (recovery phase). At each time point, the sacrificed animals were euthanized, and the lungs were harvested, fixed in formalin, and embedded in paraffin.

Sections of the lung tissues were cut on a microtome at 4 µm onto MirrIR low-e microscope slides (Kevley Technologies, Ohio), suitable for reflection-mode infrared imaging. These were then dewaxed prior to FT-IR imaging using serial washes with xylene followed by washes with ethanol[105]. Adjacent sections were cut onto regular glass slides and stained with hematoxylin and eosin (H&E) and Masson's trichrome (MT) by the Pathology Core Facility (University of Illinois–Chicago). The stained sections were

later scanned using Aperio Scanscope CS and were examined with the help of a pathologist to identify the inflammatory cells, based on H&E staining, and the collagen deposition, based on MT staining.

6.2 Infrared microspectroscopic imaging:

Infrared hyperspectral images of the lung tissues were acquired in reflectance mode using a Cary 600 Series FTIR spectrometer coupled with a Cary 600 Series microscope with a 128x128 focal plane array detector (Agilent Technologies, Santa Clara, California). Scanning was performed in the spectral range of 856 cm^{-1} to 3853 cm^{-1} , at a spectral resolution of 4 cm^{-1} , and taking the average of 8 co-scans to acquire the spectrum with a high signal-to-noise ratio. The 15X objective was used, providing a pixel size of approximately $5.5 \times 5.5\ \mu\text{m}$.

6.3. Spectral pre-processing:

The FT-IR scan data was processed using the ENVI+IDL software package (Exelis Inc., Boulder, CO). Multipoint linear baseline correction was performed on all the data, and a threshold filter based on absorbance at the 1650 cm^{-1} (Amide 1) peak was applied to exclude non-tissue pixels from analysis. The spectra were then normalized to their absorbance at 1650 cm^{-1} (Amide 1) to correct for differences in the thickness of the tissue and concentration across all the samples.

6.4 K-means cluster analysis:

Using MATLAB (MathWorks, Natick, MA), the entire sample set was then subjected to k-means cluster analysis using the Euclidean distance metric to search for natural divisions or segmentation of the tissue on the basis of the spectral data. The k-means analysis was attempted with different values of k (or numbers of clusters/partitions), and the results were compared to the light microscopy images of the adjacent H&E and MT tissue sections to see if the division appeared to correspond to any anatomical features of the lung.

6.5 Spectral analysis of normal and anomalous regions of the lung:

In addition to the cluster image analysis, regions of interest (ROIs) each were manually drawn in the regions of the lung and anomalous areas of all the lung samples, guided by the adjacent H&E and MT sections. Multiple ROIs were drawn per disease state per lung to obtain a representation of the intrasample heterogeneity present in the tissues during analysis. Averaged IR spectra in the fingerprint region (900–1,800 cm^{-1}) were then extracted for each of the ROIs (about 10,000 pixels) and subjected to second-order differentiation. These extracted, pre-processed spectra were then subjected to spectral ratio and multivariate analysis. Multiple peak absorbance ratios previously described in the literature were computed from the processed spectra. These included ratios associated with collagen (1232 cm^{-1} /1336 cm^{-1}) [111], glycosylation (1030 cm^{-1} /1080 cm^{-1}) [112] and protein (1654 cm^{-1} /1554 cm^{-1}) [113]. These ratios were then subjected to one-way analysis of variance (ANOVA) using the statistical software GraphPad Prism (GraphPad Software, Inc).

6.6 PCA-LDA analysis:

PCA-LDA analysis was performed using SPSS-24 (SPSS Inc., Chicago, Illinois) and the associated plots were made in Origin (OriginLab Corporation, Northampton, MA).

The entirety of the spectral fingerprint region from the same spectra was also analyzed using the multivariate analysis technique of principal component analysis (PCA) coupled with linear discriminant analysis (LDA). This approach was intended to convert the large dataset (232 variables per spectrum) to a smaller set of representative variables known as principal components through PCA, so that the new dataset would reflect as much of the variability in the original data as possible, while minimizing redundancy. LDA would then map the PCA data onto a set of axes designed to maximize interclass variability and minimize intra class variability, to clarify whether the samples from each time point were

in fact more different from each other than from themselves (i.e. both samples from the same time points and the other ROIs within the same sample).

7. RESULTS AND DISCUSSIONS

7.1 K-Means Analysis:

K-means analysis ultimately separated the pixels from clusters or groups based on their spectral information, representative of their biochemical state. Light microscopy examination of the H&E and MT sections from each time point suggested that this spectral segmentation corresponded to features of normal lung paryenchyma, inflammation, and fibrosis from the samples across the five timepoints (**Figure 17**).

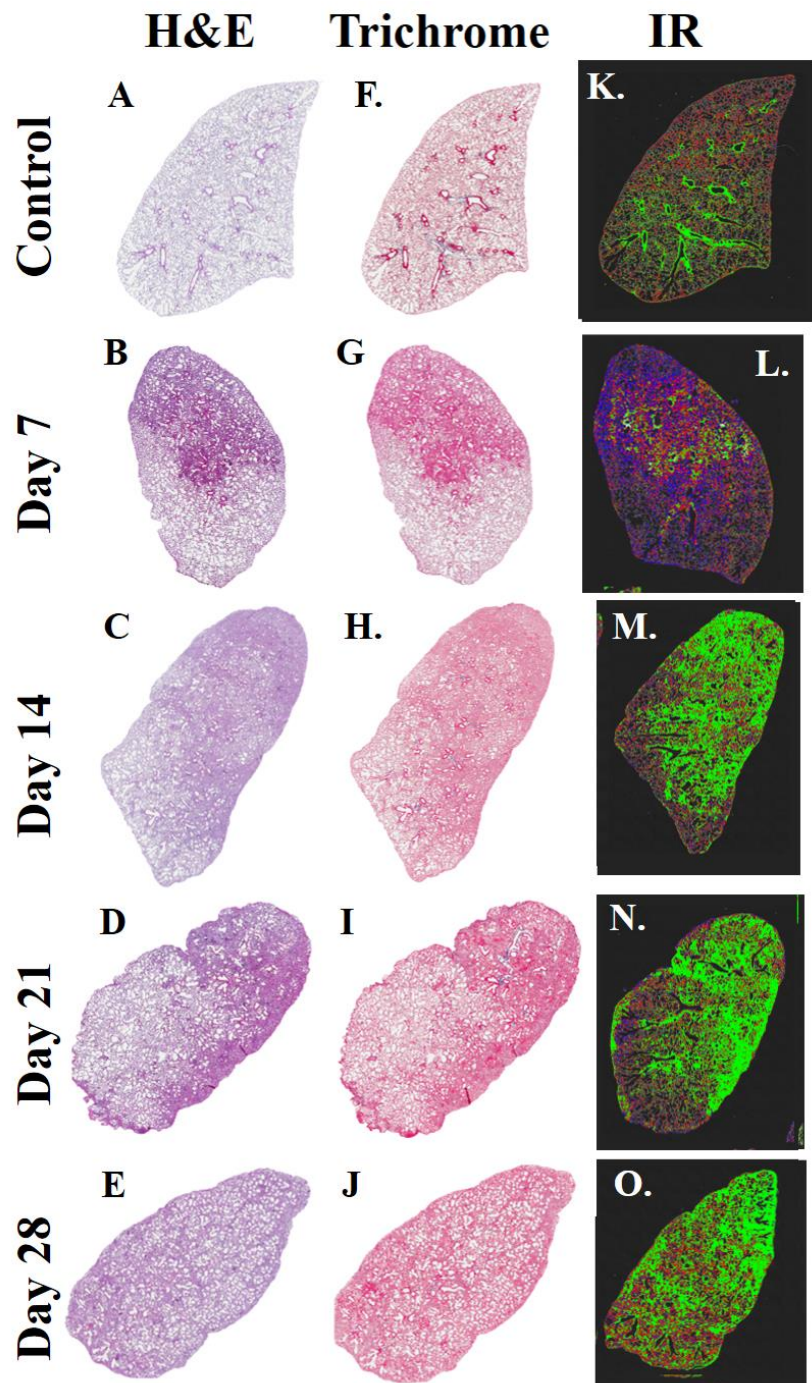


Figure.17: Array of representative tissue section examined by infrared microscopy (A-E) Brightfield images of the parallel section stained with H&E (F-J) Brightfield images of parallel tissue section stained using the Masson's trichrome. (K-O) Infrared observation of the parallel section from the tissue based on k-Means clustering image. 6 clusters were computed from a full band ($900\text{--}1800\text{ cm}^{-1}$) of the infrared absorbance dataset.

Figures 18 and 18B illustrate how the different clusters were distributed across all samples from all time points. One of the clusters (red cluster) predominated in the control samples, and was present in the background of other samples, especially at the Day 28 time point, at which point recovery from the insult is expected; this cluster could represent areas with the chemical composition of normal or healthy non-fibrotic or non-inflammatory lung tissue. By the day 7 time point, this original cluster diminished in prominence, and was replaced by other clusters, mainly the blue cluster. This change may be taken to correspond to the inflammatory changes observed at this stage of the bleomycin model, namely hypercellularity of interstitium due to increased type I pneumocytes and infiltration by polymorphonuclear leukocytes.

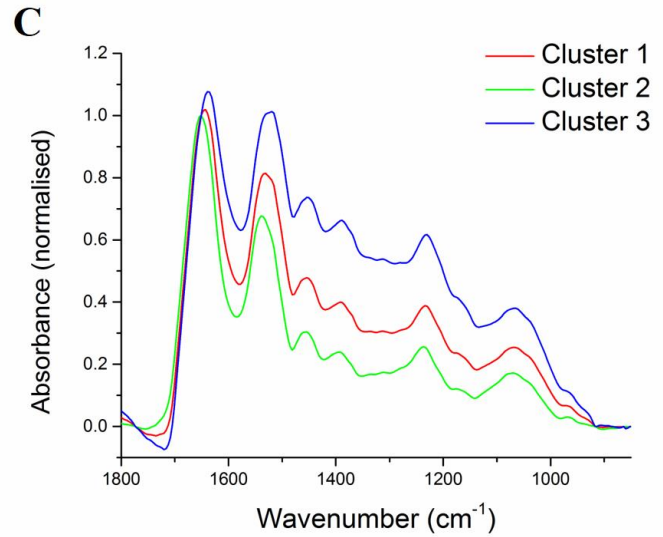
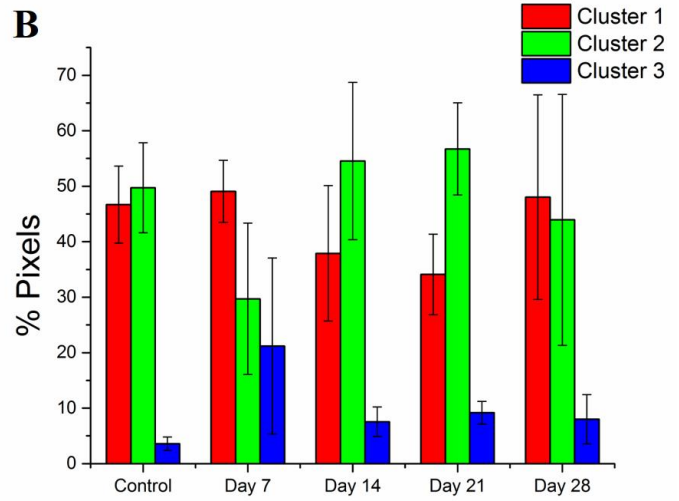
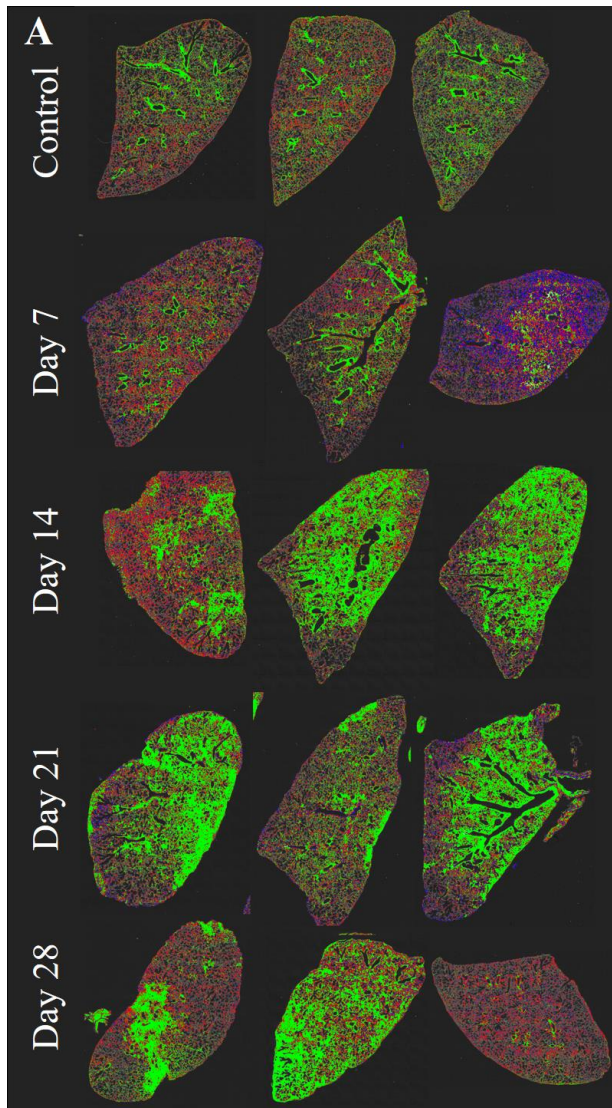


Figure.18: Non-hierarchical k-means cluster analysis depicting the histopathological regions of each lung across different groups (A) k-Means clustering image (3 clusters) of the lung tissues from each group calculated from a full band (900–1800 cm^{-1}) infrared absorbance dataset. (B) Mean absorption spectra calculated from each cluster, which is quantified as seen in (C).

In the Day 14 samples, the original cluster 2 (potentially healthy tissue) is further diminished and replaced largely by an increase in another cluster (green cluster). The green cluster might be the fibrous or fibrotic regions of the lung. Histologically, this stage would show an increased presence of macrophages and chronic inflammatory cells. By Day 21, there is a substantial increase in the new green cluster, which may be taken to be a spectroscopic correlate to the increased collagen deposition evident by histology, in addition to the other inflammatory markers present. Finally, by Day 28, the green cluster falls off and there is a resurgence of the original cluster 2, while there is some persistence of the green cluster that predominated during the early phases of damage. This may indicate the recovery phase of the model, in which fibrosis is healed, but there is still diffuse lymphocytic clustering in the interstitium and macrophages encompassing alveolar cells.

While a rigorous assignment of each cluster to a particular tissue feature or cell type was not performed, the results of the k-means analysis suggest that the spectroscopic data collected through FT-IR detect the pathological changes occurring at different phases of the bleomycin damage model. Comparison of the k-means maps to the H&E and MT stained adjacent sections indicated a fairly good agreement between these techniques as to the presence and distribution of changes across the lungs over time.

In sum, these results offer evidence that FT-IR imaging is sensitive to the pathologic processes at work in this model; **Figure 18C** shows that each of the clusters has a different spectral profile, which in turn indicates a different biochemical composition stemming from different cellular components and metabolic processes taking place.

7.2 Spectral analysis of normal and anomalous regions of the lung:

The average, processed spectra extracted from manual ROIs in fibrotic and non-fibrotic regions of all the samples (total of 10 fibrotic and 10 non-fibrotic per lung) are presented in **Figure 19**. Variations in

absorbance at different bands were seen between fibrotic and non-fibrotic regions as well as between the different time points, both in the original spectra and in their second derivatives.

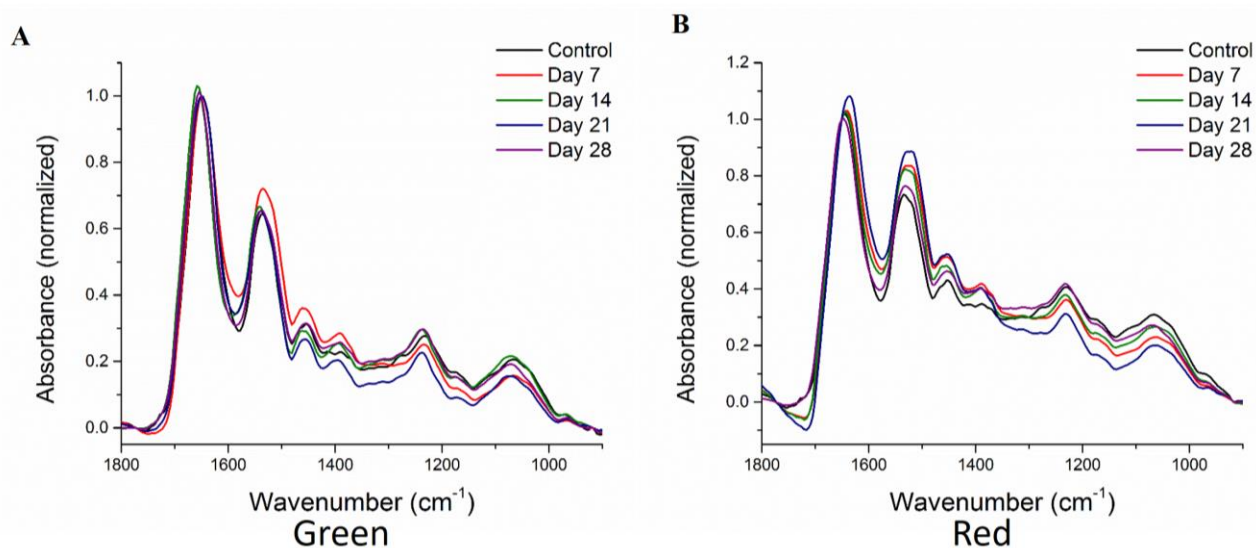


Figure 19: Spectral data were extracted from the normal (red) and anomalous (green) of the IR image scans. The average spectra for different stages of fibrosis in the (A) anomalous and (B) normal regions of the lung tissue showing a significant variation in certain spectral points of the IR spectra. The second derivative of the absorption spectra in (C) fibrotic and (D) non-fibrotic regions.

7.3 Ratiometric Analysis:

Ratiometric analysis on these spectra were performed for the collagen ($1232\text{ cm}^{-1}/1336\text{ cm}^{-1}$) [111], glycosylation [112] and protein ($1654\text{ cm}^{-1}/1554\text{ cm}^{-1}$) [113]. ANOVA analysis of these ratios showed

that in most cases, there was a statistically significant change in these ratios between adjacent time points, both among the fibrotic regions and the non-fibrotic regions (**Figure 20**). The inferences have been made using multiple observations per sample, and therefore ANOVA has not been performed on the samples themselves.

The ratio of spectral bands 1232 cm^{-1} and 1336 cm^{-1} (amide III to the collagen CH_2 side chain vibrations) is thought to represent changes in collagen in tissue [111]. In the green areas, this ratio decreased at Day 7 but then appeared to peak at Day 21, when the model demonstrated the most fibrotic changes, and a similar trend was seen in non-fibrotic tissues (**Figure 20A and 20B**). These changes may relate to deposition of abnormal collagen, different in structure and composition from the collagen normally present in this tissue. This would be reasonable to expect in the areas of fibrosis, and it may be true to a lesser extent in the tissue areas which are not grossly fibrotic, reflecting the dysregulated response of fibroblasts to cytokines mediating the disease process.

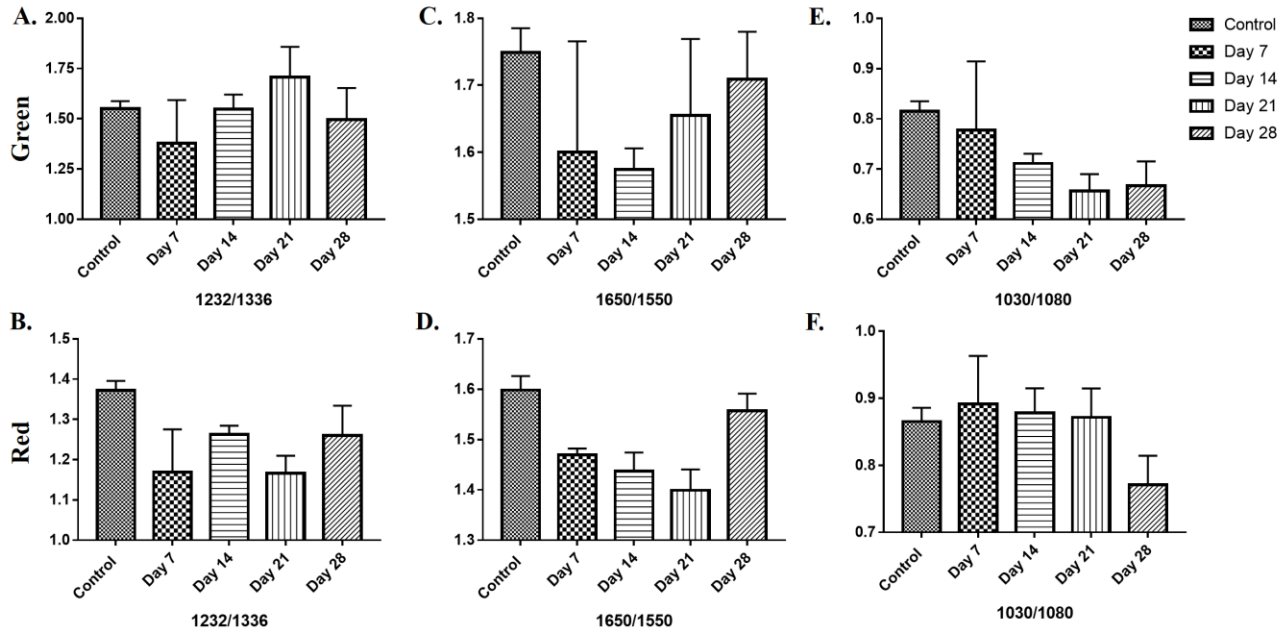


Figure 20: Ratiometric analysis of the IR spectra. The ratio of intensities at 1232/1336 gives the collagen map in the tissue for (A) anomalous (green) and (B) normal (red) regions. The spectral ratio of 1654/1554 in (C) fibrotic and (D) non-fibrotic regions indicates not only any changes in the structural rearrangements of the existing proteins, but also the expression of a new proteins with varied structural characteristics. Glycosylation patterns across the lung tissue are interpreted using 1080/1030 spectral ratio in (E) fibrotic and (F) non-fibrotic regions.

Glycosylation is another important biochemical process in tissue, which can manifest spectroscopically through changes of the $1030\text{ cm}^{-1}/1080\text{ cm}^{-1}$ absorbance ratio as shown in **Figure 20 E and 20F** [112]. The absorbance at 1030 cm^{-1} represents the glycogen COH deformation, whereas 1080 cm^{-1} represents the glycogen C-C stretch, and their ratio in fibrotic regions gradually decreased from control to Day 21 and increased on Day 28 (**Figure 20 E**). Glycosylation is essential for cell migration [114], which is a central mechanism of PF because the infiltration of inflammatory cells into interstitial lung spaces promotes

fibrosis. In addition, glycosylation of the extracellular domain of TGF- β receptors also induces stimulation of the TGF-beta which is an important signaling pathway mediating fibrosis [115].

Finally, a band ratio examining the spectral changes in the protein regions was also processed. The absorbance at 1654 cm^{-1} represents the protein C=O stretching of the structural protein (amide I), whereas 1545 cm^{-1} represents the N-H bending and C-N stretching of the polypeptides and protein background (amide II). Changes in the ratio $1654\text{ cm}^{-1}/1545\text{ cm}^{-1}$ may correspond to changes in the structural rearrangements of existing proteins or the expression of new proteins with varied structural characteristics. In both fibrotic and nonfibrotic regions, this ratio decreased at Day 7 and then increased on the following days in the fibrotic regions (**Figure 20 C and 20 D**). These changes could be due to a shift from the neutrophilic activity in Day 7 to the deposition of ECM proteins like elastin, fibronectin, and laminin that predominate in later time points with the development of fibrosis [116].

7.4 Multivariate analysis:

Moving from the ratiometric analysis of the fibrotic and nonfibrotic areas to multivariate analysis, PC-LDA analysis was able to distinguish the different time points of the bleomycin challenge, with the areas from the samples of the same time point clustering together (**Figure 21**). The separation of the observations by time point suggests a difference in biochemical composition (as measured by the spectral signature) over time. Interestingly, the values of the first LD for both fibrotic and nonfibrotic areas varied with the time course, with increasing time points moving further from control, with the exception of Day 28, which most closely resembled the control samples.

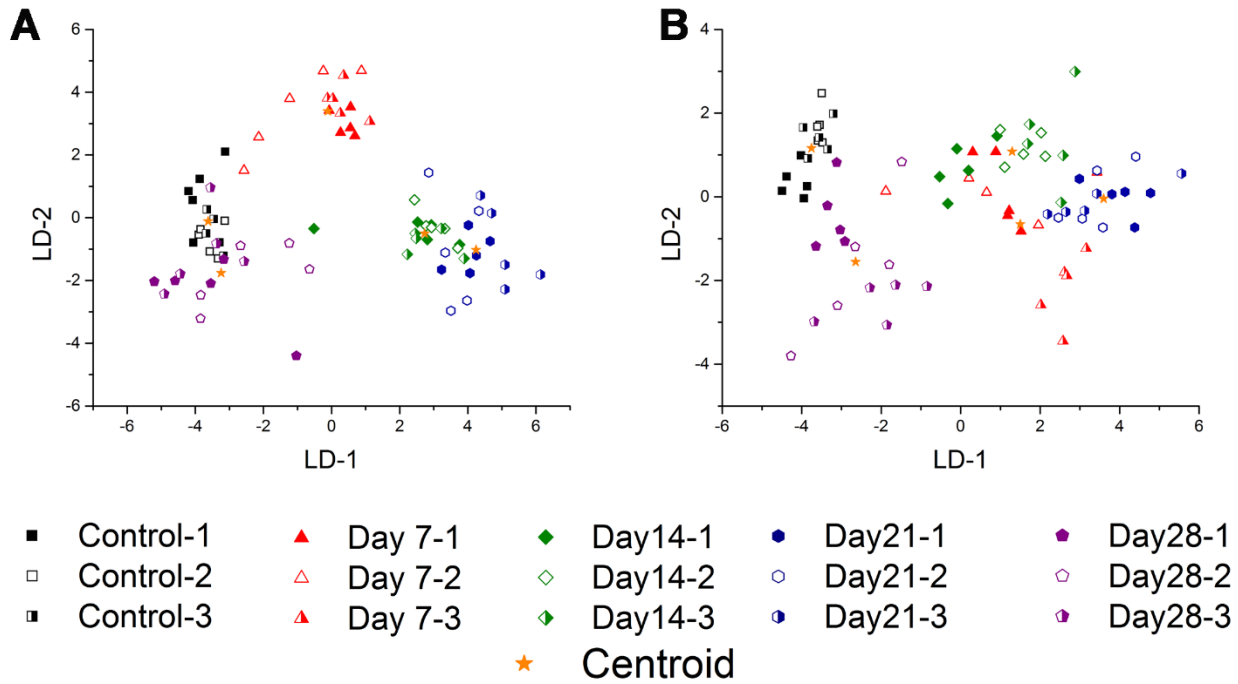


Figure 21: PCA-LDA analysis could classify the different groups with varying stages of fibrosis based on IR data from (A, C, E) anomalous and (B, D, F) normal regions of the lung tissue, enabling clear distinction of the pathological states of fibrosis.

While a precise interpretation cannot be assigned, the course would suggest that the spectral signature from both fibrotic and nonfibrotic tissues changes with the pathologies being developed in the model. Inflammation predominates in Day 7, with an influx of inflammatory cells and profibrotic cytokines that transform the healthy control lung. There is parallel development of fibrosis, due to activation of cells in lungs which lead to the deposition of extracellular matrix components, further perturbing the biochemical composition and spectral characteristics of the tissue. By day 28, there is recovery, and the biochemical composition returns to the baseline at control. The quantitative results of classification of time point by

PC-LDA is given in Table 1; however, this classification did not utilize cross-validation, or a separate validation set.

8. CONCLUSION

The current study applies FT-IR imaging to the detection of biochemical changes in a murine model of bleomycin-induced pulmonary fibrosis. Based on k-means clustering analysis, the IR dataset reveals biochemical changes across the spatial features of lung tissue that may correspond to the morphological changes that are seen by routine histology. This suggests that the underlying chemical processes that give rise to structural changes are accessible to this imaging modality.

Furthermore, the spectral changes in both fibrotic and non-fibrotic regions throughout the time course of the model, as evidenced by both the spectral ratios and PC-LDA analysis, suggest that FT-IR imaging can assess how the biochemical status, and therefore the disease state, of the lung tissue is perturbed by the process of fibrosis, and how it returns to a healthy baseline.

These two features of the technique, the ability to detect chemical changes across the geography of a tissue and to monitor the disease state of the tissue over time, are the first steps in developing this modality as a tool for the study of IPF. The capacity to locate areas of lung tissue that are undergoing biochemical change can help assess other models of the disease, while sensitivity to disease progression and recovery offers utility in therapeutic investigations.

Further work will need to characterize the biochemical changes being detected and assess whether any of these spectral markers are present prior to the manifestation of a morphological changes. More importantly, future studies will translate these findings from the murine bleomycin model to human control and IPF tissues and correlate them to clinical outcomes such as six-minute walk tests and response to novel therapeutic agents. With further investigations, FT-IR imaging holds the potential to be a powerful adjunct to current histopathological techniques in finding better ways to understand and manage this disease.

8.1 Future directions:

As an extension of the current study, the IR data from the current study could be further extrapolated to classify the lung tissue in each group to epithelial, mesenchymal cells, fibroblasts & myofibroblasts; collagen deposition in the lung tissue, thereby identifying the epithelial to mesenchymal transition during different stages of fibrosis, for which single-instillation of bleomycin induced PF is a very good preclinical model. Similar to the IR study of the fibrotic lung in mice, the studies would be extended to human tissues and IR images of the control and IPF lung will be acquired and the biochemical changes across both the groups would be studied. This technique could also be used to differentiate between IPF and other diseases part of the ILD family, which have similar features making it a challenge for the clinicians to diagnose the disease. IR imaging will provide the pulmonary fibrosis community a novel tool to aid in diagnosis, in conjugation to the currently existing histopathological techniques.

SUMMARY OF THE STUDY

Idiopathic pulmonary fibrosis (IPF) is a detrimental lung disease characterized by alveolar epithelial apoptosis, dysregulated repair of epithelial injury, scar formation and respiratory failure. There is epithelial dysfunction, followed by epithelial to mesenchymal transition and fibroblasts to myofibroblasts differentiation, all of which contribute to extracellular matrix deposition in the lung. The current scenario warrants for identification of effective therapeutic targets for the treatment of IPF. Using bleomycin induced pulmonary fibrosis model, phospholipase D was found to be an important therapeutic target in IPF based on histological analysis and several other biochemical assays. Further it was found that phospholipase D mediates fibrogenesis by regulating mitochondrial dysfunction mediated apoptosis in epithelial cells using *in vitro* analysis.

Another approach to understand the changes in the lung during different stages of fibrosis was Fourier-transform infrared imaging, which is a label free imaging technique to assess the biochemical changes in the lung across different stages of fibrosis. The IR images could distinguish the different stages of the disease as well as give precise information of alteration of specific biomolecules in the lung across different stages of fibrosis. Having validated this technique for the study of lung fibrosis, this technique could further be used to assess novel genetically modified animal models for their efficacy as a therapeutic strategy in IPF and it could also be used to study different mechanisms in IPF like EMT by extrapolating the biochemical information from all the cell types in the lung simultaneously using IR. Thus, this study not only employs the currently existing tools and techniques for identifying and validating a new therapeutic target against IPF, but also presents a novel technique like FT-IR that will aid in elucidating the signaling mechanisms mediating fibrosis.

BIBLIOGRAPHY

1. Antoniou, K.M., et al., *Interstitial lung disease*. Eur Respir Rev, 2014. **23**(131): p. 40-54.
2. Sgalla, G., A. Biffi, and L. Richeldi, *Idiopathic pulmonary fibrosis: Diagnosis, epidemiology and natural history*. Respirology, 2016. **21**(3): p. 427-37.
3. Martinez, F.J., et al., *Idiopathic pulmonary fibrosis*. Nature Reviews Disease Primers, 2017. **3**: p. 17074.
4. Ryu, J.H., et al., *Idiopathic pulmonary fibrosis: evolving concepts*. Mayo Clin Proc, 2014. **89**(8): p. 1130-42.
5. Daba, M.H., et al., *Drug-induced pulmonary fibrosis*. Saudi Med J, 2004. **25**(6): p. 700-6.
6. Samara, K.D., et al., *Smoking and pulmonary fibrosis: novel insights*. Pulm Med, 2011. **2011**: p. 461439.
7. Evans, C.M., et al., *Idiopathic Pulmonary Fibrosis: A Genetic Disease That Involves Mucociliary Dysfunction of the Peripheral Airways*. Physiol Rev, 2016. **96**(4): p. 1567-91.
8. Cottin, V. and L. Richeldi, *Neglected evidence in idiopathic pulmonary fibrosis and the importance of early diagnosis and treatment*. Eur Respir Rev, 2014. **23**(131): p. 106-10.
9. Rossi, G. and P. Spagnolo, *Biopsy in idiopathic pulmonary fibrosis: back to the future*. Expert Rev Respir Med, 2017. **11**(9): p. 679-684.
10. Olson, A.L., et al., *Tracking dyspnea up to supplemental oxygen prescription among patients with pulmonary fibrosis*. BMC Pulm Med, 2017. **17**(1): p. 152.
11. Mogulkoc, N., et al., *Pulmonary function in idiopathic pulmonary fibrosis and referral for lung transplantation*. Am J Respir Crit Care Med, 2001. **164**(1): p. 103-8.
12. Raghu, G. and M. Selman, *Nintedanib and pirfenidone. New antifibrotic treatments indicated for idiopathic pulmonary fibrosis offer hopes and raises questions*. Am J Respir Crit Care Med, 2015. **191**(3): p. 252-4.
13. George, T.J., G.J. Arnaoutakis, and A.S. Shah, *Lung transplant in idiopathic pulmonary fibrosis*. Arch Surg, 2011. **146**(10): p. 1204-9.
14. Cummings, R., et al., *Phospholipase D/phosphatidic acid signal transduction: role and physiological significance in lung*. Mol Cell Biochem, 2002. **234-235**(1-2): p. 99-109.
15. Liu, Y., Y. Su, and X. Wang, *Phosphatidic acid-mediated signaling*. Adv Exp Med Biol, 2013. **991**: p. 159-76.
16. Gaits, F., et al., *Lysophosphatidic acid as a phospholipid mediator: pathways of synthesis*. FEBS Lett, 1997. **410**(1): p. 54-8.
17. Huang, K.P., *The mechanism of protein kinase C activation*. Trends Neurosci, 1989. **12**(11): p. 425-32.
18. Natarajan, V., *Phospholipase D and signal transduction in mammalian cells*. Chem Phys Lipids, 1996. **80**(1-2): p. 1-2.
19. Liscovitch, M., et al., *Phospholipase D: molecular and cell biology of a novel gene family*. Biochem J, 2000. **345 Pt 3**: p. 401-15.
20. Nelson, R.K. and M.A. Frohman, *Physiological and pathophysiological roles for phospholipase D*. J Lipid Res, 2015. **56**(12): p. 2229-37.
21. Frohman, M.A., *The phospholipase D superfamily as therapeutic targets*. Trends Pharmacol Sci, 2015. **36**(3): p. 137-44.
22. Parmentier, J.H., et al., *Phospholipase D activation by norepinephrine is mediated by 12(s)-, 15(s)-, and 20-hydroxyeicosatetraenoic acids generated by stimulation of cytosolic phospholipase a2. tyrosine phosphorylation of phospholipase d2 in response to norepinephrine*. J Biol Chem, 2001. **276**(19): p. 15704-11.
23. Scott, S.A., et al., *Design of isoform-selective phospholipase D inhibitors that modulate cancer cell invasiveness*. Nat Chem Biol, 2009. **5**(2): p. 108-17.

24. Bruntz, R.C., C.W. Lindsley, and H.A. Brown, *Phospholipase D signaling pathways and phosphatidic acid as therapeutic targets in cancer*. *Pharmacol Rev*, 2014. **66**(4): p. 1033-79.
25. Jenkins, G.M. and M.A. Frohman, *Phospholipase D: a lipid centric review*. *Cell Mol Life Sci*, 2005. **62**(19-20): p. 2305-16.
26. Osisami, M., W. Ali, and M.A. Frohman, *A role for phospholipase D3 in myotube formation*. *PLoS One*, 2012. **7**(3): p. e33341.
27. Gonzalez, A.C., et al., *Unconventional Trafficking of Mammalian Phospholipase D3 to Lysosomes*. *Cell Rep*, 2018. **22**(4): p. 1040-1053.
28. Yoshikawa, F., et al., *Phospholipase D family member 4, a transmembrane glycoprotein with no phospholipase D activity, expression in spleen and early postnatal microglia*. *PLoS One*, 2010. **5**(11): p. e13932.
29. Gao, L., et al., *PLD4 promotes M1 macrophages to perform antitumor effects in colon cancer cells*. *Oncol Rep*, 2017. **37**(1): p. 408-416.
30. Chiba, T., et al., *Microglial phospholipase D4 deficiency influences myelination during brain development*. *Proc Jpn Acad Ser B Phys Biol Sci*, 2016. **92**(7): p. 237-54.
31. Terao, C., et al., *PLD4 as a novel susceptibility gene for systemic sclerosis in a Japanese population*. *Arthritis Rheum*, 2013. **65**(2): p. 472-80.
32. Trivedi, P., et al., *Targeting Phospholipase D4 Attenuates Kidney Fibrosis*. *J Am Soc Nephrol*, 2017. **28**(12): p. 3579-3589.
33. Anney, R., et al., *A genome-wide scan for common alleles affecting risk for autism*. *Hum Mol Genet*, 2010. **19**(20): p. 4072-82.
34. Kabayama, Y., et al., *Roles of MIWI, MILI and PLD6 in small RNA regulation in mouse growing oocytes*. *Nucleic Acids Res*, 2017. **45**(9): p. 5387-5398.
35. Chen, Y., et al., *Glycerol kinase-like proteins cooperate with Pld6 in regulating sperm mitochondrial sheath formation and male fertility*. *Cell Discov*, 2017. **3**: p. 17030.
36. Gao, Q. and M.A. Frohman, *Roles for the lipid-signaling enzyme MitoPLD in mitochondrial dynamics, piRNA biogenesis, and spermatogenesis*. *BMB Rep*, 2012. **45**(1): p. 7-13.
37. Gobel, K., et al., *Phospholipase D1 mediates lymphocyte adhesion and migration in experimental autoimmune encephalomyelitis*. *Eur J Immunol*, 2014. **44**(8): p. 2295-305.
38. Oguin, T.H., 3rd, et al., *Phospholipase D facilitates efficient entry of influenza virus, allowing escape from innate immune inhibition*. *J Biol Chem*, 2014. **289**(37): p. 25405-17.
39. Oliveira, T.G. and G. Di Paolo, *Phospholipase D in brain function and Alzheimer's disease*. *Biochim Biophys Acta*, 2010. **1801**(8): p. 799-805.
40. Henkels, K.M., et al., *Phospholipase D (PLD) drives cell invasion, tumor growth and metastasis in a human breast cancer xenograph model*. *Oncogene*, 2013. **32**(49): p. 5551-62.
41. Brown, H.A., P.G. Thomas, and C.W. Lindsley, *Targeting phospholipase D in cancer, infection and neurodegenerative disorders*. *Nat Rev Drug Discov*, 2017. **16**(5): p. 351-367.
42. Zhu, X., et al., *The role of phospholipase D1 in liver fibrosis induced by dimethylnitrosamine in vivo*. *Dig Dis Sci*, 2014. **59**(8): p. 1779-88.
43. Yamamoto, K., et al., *N-methylethanolamine attenuates cardiac fibrosis and improves diastolic function: inhibition of phospholipase D as a possible mechanism*. *Eur Heart J*, 2004. **25**(14): p. 1221-9.
44. Patel, R.B., et al., *Pulmonary fibrosis inducer, bleomycin, causes redox-sensitive activation of phospholipase D and cytotoxicity through formation of bioactive lipid signal mediator, phosphatidic acid, in lung microvascular endothelial cells*. *Int J Toxicol*, 2011. **30**(1): p. 69-90.
45. Usatyuk, P.V., et al., *Phospholipase D signaling mediates reactive oxygen species-induced lung endothelial barrier dysfunction*. *Pulm Circ*, 2013. **3**(1): p. 108-15.
46. Pardo, A. and M. Selman, *Lung Fibroblasts, Aging, and Idiopathic Pulmonary Fibrosis*. *Ann Am Thorac Soc*, 2016. **13**(Supplement_5): p. S417-S421.

47. Jayachandran, A., et al., *SNAI transcription factors mediate epithelial-mesenchymal transition in lung fibrosis*. Thorax, 2009. **64**(12): p. 1053-61.
48. Kim, S.J., et al., *The Role of Mitochondrial DNA in Mediating Alveolar Epithelial Cell Apoptosis and Pulmonary Fibrosis*. Int J Mol Sci, 2015. **16**(9): p. 21486-519.
49. Liu, X. and Z. Chen, *The pathophysiological role of mitochondrial oxidative stress in lung diseases*. J Transl Med, 2017. **15**(1): p. 207.
50. Jablonski, R.P., et al., *SIRT3 deficiency promotes lung fibrosis by augmenting alveolar epithelial cell mitochondrial DNA damage and apoptosis*. FASEB J, 2017. **31**(6): p. 2520-2532.
51. B, B.M., et al., *Animal models of fibrotic lung disease*. Am J Respir Cell Mol Biol, 2013. **49**(2): p. 167-79.
52. Mouratis, M.A. and V. Aidinis, *Modeling pulmonary fibrosis with bleomycin*. Curr Opin Pulm Med, 2011. **17**(5): p. 355-61.
53. Matute-Bello, G., et al., *An official American Thoracic Society workshop report: features and measurements of experimental acute lung injury in animals*. Am J Respir Cell Mol Biol, 2011. **44**(5): p. 725-38.
54. Hubner, R.H., et al., *Standardized quantification of pulmonary fibrosis in histological samples*. Biotechniques, 2008. **44**(4): p. 507-11, 514-7.
55. Kim, S.J., et al., *Mitochondria-targeted Ogg1 and aconitase-2 prevent oxidant-induced mitochondrial DNA damage in alveolar epithelial cells*. J Biol Chem, 2014. **289**(9): p. 6165-76.
56. Oliveira, T.G., et al., *Phospholipase d2 ablation ameliorates Alzheimer's disease-linked synaptic dysfunction and cognitive deficits*. J Neurosci, 2010. **30**(49): p. 16419-28.
57. Shaghghi, H., et al., *Metabolic spectroscopy of inflammation in a bleomycin-induced lung injury model using hyperpolarized 1-(13) C pyruvate*. NMR Biomed, 2014. **27**(8): p. 939-47.
58. Xiao, J., et al., *miR-29 inhibits bleomycin-induced pulmonary fibrosis in mice*. Mol Ther, 2012. **20**(6): p. 1251-60.
59. Hur, J.H., et al., *Phospholipase D1 deficiency in mice causes nonalcoholic fatty liver disease via an autophagy defect*. Sci Rep, 2016. **6**: p. 39170.
60. Kim, S.J., et al., *Mitochondrial catalase overexpressed transgenic mice are protected against lung fibrosis in part via preventing alveolar epithelial cell mitochondrial DNA damage*. Free Radic Biol Med, 2016. **101**: p. 482-490.
61. Usatyuk, P.V., et al., *Phospholipase D-mediated activation of IQGAP1 through Rac1 regulates hyperoxia-induced p47phox translocation and reactive oxygen species generation in lung endothelial cells*. J Biol Chem, 2009. **284**(22): p. 15339-52.
62. King, T.E., Jr., A. Pardo, and M. Selman, *Idiopathic pulmonary fibrosis*. Lancet, 2011. **378**(9807): p. 1949-61.
63. Ozden, O., et al., *Acetylation of MnSOD directs enzymatic activity responding to cellular nutrient status or oxidative stress*. Aging (Albany NY), 2011. **3**(2): p. 102-7.
64. Zank, D.C., et al., *Idiopathic Pulmonary Fibrosis: Aging, Mitochondrial Dysfunction, and Cellular Bioenergetics*. Front Med (Lausanne), 2018. **5**: p. 10.
65. Zoz, D.F., W.E. Lawson, and T.S. Blackwell, *Idiopathic pulmonary fibrosis: a disorder of epithelial cell dysfunction*. Am J Med Sci, 2011. **341**(6): p. 435-8.
66. Itoh, T., et al., *The tyrosine kinase Fer is a downstream target of the PLD-PA pathway that regulates cell migration*. Sci Signal, 2009. **2**(87): p. ra52.
67. Foster, D.A. and L. Xu, *Phospholipase D in cell proliferation and cancer*. Mol Cancer Res, 2003. **1**(11): p. 789-800.
68. Ali, W.H., et al., *Deficiencies of the lipid-signaling enzymes phospholipase D1 and D2 alter cytoskeletal organization, macrophage phagocytosis, and cytokine-stimulated neutrophil recruitment*. PLoS One, 2013. **8**(1): p. e55325.

69. Pendyala, S., et al., *Regulation of NADPH oxidase in vascular endothelium: the role of phospholipases, protein kinases, and cytoskeletal proteins*. *Antioxid Redox Signal*, 2009. **11**(4): p. 841-60.
70. Cazzolli, R., et al., *Phospholipid signalling through phospholipase D and phosphatidic acid*. *IUBMB Life*, 2006. **58**(8): p. 457-61.
71. Brindley, D.N. and C. Pilquill, *Lipid phosphate phosphatases and signaling*. *J Lipid Res*, 2009. **50 Suppl**: p. S225-30.
72. Zhang, L., et al., *Interleukin-7 and transforming growth factor-beta play counter-regulatory roles in protein kinase C-delta-dependent control of fibroblast collagen synthesis in pulmonary fibrosis*. *J Biol Chem*, 2004. **279**(27): p. 28315-9.
73. Chichger, H., et al., *PKC delta and beta11 regulate angiotensin II-mediated fibrosis through p38: a mechanism of RV fibrosis in pulmonary hypertension*. *Am J Physiol Lung Cell Mol Physiol*, 2015. **308**(8): p. L827-36.
74. Luzina, I.G., et al., *PKCalpha mediates CCL18-stimulated collagen production in pulmonary fibroblasts*. *Am J Respir Cell Mol Biol*, 2006. **35**(3): p. 298-305.
75. Huang, L.S., et al., *Lysophosphatidic acid receptor-2 deficiency confers protection against bleomycin-induced lung injury and fibrosis in mice*. *Am J Respir Cell Mol Biol*, 2013. **49**(6): p. 912-22.
76. Eder, A.M., et al., *Constitutive and lysophosphatidic acid (LPA)-induced LPA production: role of phospholipase D and phospholipase A2*. *Clin Cancer Res*, 2000. **6**(6): p. 2482-91.
77. Sonoda, H., et al., *A novel phosphatidic acid-selective phospholipase A1 that produces lysophosphatidic acid*. *J Biol Chem*, 2002. **277**(37): p. 34254-63.
78. Knowlden, S. and S.N. Georas, *The autotaxin-LPA axis emerges as a novel regulator of lymphocyte homing and inflammation*. *J Immunol*, 2014. **192**(3): p. 851-7.
79. Oikonomou, N., et al., *Pulmonary autotaxin expression contributes to the pathogenesis of pulmonary fibrosis*. *Am J Respir Cell Mol Biol*, 2012. **47**(5): p. 566-74.
80. Tager, A.M., et al., *The lysophosphatidic acid receptor LPA1 links pulmonary fibrosis to lung injury by mediating fibroblast recruitment and vascular leak*. *Nat Med*, 2008. **14**(1): p. 45-54.
81. Black, K.E., et al., *Autotaxin activity increases locally following lung injury, but is not required for pulmonary lysophosphatidic acid production or fibrosis*. *FASEB J*, 2016. **30**(6): p. 2435-50.
82. Uttara, B., et al., *Oxidative stress and neurodegenerative diseases: a review of upstream and downstream antioxidant therapeutic options*. *Curr Neuropharmacol*, 2009. **7**(1): p. 65-74.
83. Ray, P.D., B.W. Huang, and Y. Tsuji, *Reactive oxygen species (ROS) homeostasis and redox regulation in cellular signaling*. *Cell Signal*, 2012. **24**(5): p. 981-90.
84. Walters, D.M., H.Y. Cho, and S.R. Kleeberger, *Oxidative stress and antioxidants in the pathogenesis of pulmonary fibrosis: a potential role for Nrf2*. *Antioxid Redox Signal*, 2008. **10**(2): p. 321-32.
85. Cheresh, P., et al., *Oxidative stress and pulmonary fibrosis*. *Biochim Biophys Acta*, 2013. **1832**(7): p. 1028-40.
86. Bocchino, M., et al., *Reactive oxygen species are required for maintenance and differentiation of primary lung fibroblasts in idiopathic pulmonary fibrosis*. *PLoS One*, 2010. **5**(11): p. e14003.
87. Jain, M., et al., *Mitochondrial reactive oxygen species regulate transforming growth factor-beta signaling*. *J Biol Chem*, 2013. **288**(2): p. 770-7.
88. Amara, N., et al., *NOX4/NADPH oxidase expression is increased in pulmonary fibroblasts from patients with idiopathic pulmonary fibrosis and mediates TGFbeta1-induced fibroblast differentiation into myofibroblasts*. *Thorax*, 2010. **65**(8): p. 733-8.
89. Stasek, J.E., Jr., V. Natarajan, and J.G. Garcia, *Phosphatidic acid directly activates endothelial cell protein kinase C*. *Biochem Biophys Res Commun*, 1993. **191**(1): p. 134-41.
90. Jenkins, C.M. and M.R. Waterman, *Flavodoxin and NADPH-flavodoxin reductase from Escherichia coli support bovine cytochrome P450c17 hydroxylase activities*. *J Biol Chem*, 1994. **269**(44): p. 27401-8.

91. Moritz, A., et al., *Phosphatidic acid is a specific activator of phosphatidylinositol-4-phosphate kinase*. J Biol Chem, 1992. **267**(11): p. 7207-10.
92. Delon, C., et al., *Sphingosine kinase 1 is an intracellular effector of phosphatidic acid*. J Biol Chem, 2004. **279**(43): p. 44763-74.
93. Kamp, D.W., et al., *The role of free radicals in asbestos-induced diseases*. Free Radic Biol Med, 1992. **12**(4): p. 293-315.
94. Kinnula, V.L. and J.D. Crapo, *Superoxide dismutases in the lung and human lung diseases*. Am J Respir Crit Care Med, 2003. **167**(12): p. 1600-19.
95. Chen, Y., et al., *Sirtuin-3 (SIRT3), a therapeutic target with oncogenic and tumor-suppressive function in cancer*. Cell Death Dis, 2014. **5**: p. e1047.
96. Kincaid, B. and E. Bossy-Wetzler, *Forever young: SIRT3 a shield against mitochondrial meltdown, aging, and neurodegeneration*. Front Aging Neurosci, 2013. **5**: p. 48.
97. Kim, K.C., et al., *Baicalein (5,6,7-trihydroxyflavone) reduces oxidative stress-induced DNA damage by upregulating the DNA repair system*. Cell Biol Toxicol, 2012. **28**(6): p. 421-33.
98. Guo, C., et al., *Oxidative stress, mitochondrial damage and neurodegenerative diseases*. Neural Regen Res, 2013. **8**(21): p. 2003-14.
99. Sun, K.W., et al., *Oridonin induces apoptosis in gastric cancer through Apaf-1, cytochrome c and caspase-3 signaling pathway*. World J Gastroenterol, 2012. **18**(48): p. 7166-74.
100. Tomassetti, S., et al., *The multidisciplinary approach in the diagnosis of idiopathic pulmonary fibrosis: a patient case-based review*. Eur Respir Rev, 2015. **24**(135): p. 69-77.
101. Elicker, B.M., K.G. Kallianos, and T.S. Henry, *The role of high-resolution computed tomography in the follow-up of diffuse lung disease: Number 2 in the Series "Radiology" Edited by Nicola Sverzellati and Sujal Desai*. Eur Respir Rev, 2017. **26**(144).
102. Tomassetti, S., et al., *Bronchoscopic Lung Cryobiopsy Increases Diagnostic Confidence in the Multidisciplinary Diagnosis of Idiopathic Pulmonary Fibrosis*. Am J Respir Crit Care Med, 2016. **193**(7): p. 745-52.
103. Kaarteenaho, R., *The current position of surgical lung biopsy in the diagnosis of idiopathic pulmonary fibrosis*. Respir Res, 2013. **14**: p. 43.
104. Sumida, Y., A. Nakajima, and Y. Itoh, *Limitations of liver biopsy and non-invasive diagnostic tests for the diagnosis of nonalcoholic fatty liver disease/nonalcoholic steatohepatitis*. World J Gastroenterol, 2014. **20**(2): p. 475-85.
105. Baker, M.J., et al., *Using Fourier transform IR spectroscopy to analyze biological materials*. Nat Protoc, 2014. **9**(8): p. 1771-91.
106. Nasse, M.J., et al., *High-resolution Fourier-transform infrared chemical imaging with multiple synchrotron beams*. Nat Methods, 2011. **8**(5): p. 413-6.
107. Nazeer, S.S., et al., *Infrared spectroscopic imaging: Label-free biochemical analysis of stroma and tissue fibrosis*. Int J Biochem Cell Biol, 2017. **92**: p. 14-17.
108. Jones, A.W. and N.L. Reeve, *Ultrastructural study of bleomycin-induced pulmonary changes in mice*. J Pathol, 1978. **124**(4): p. 227-33.
109. Izbicki, G., et al., *Time course of bleomycin-induced lung fibrosis*. Int J Exp Pathol, 2002. **83**(3): p. 111-9.
110. Moore, B.B. and C.M. Hogaboam, *Murine models of pulmonary fibrosis*. Am J Physiol Lung Cell Mol Physiol, 2008. **294**(2): p. L152-60.
111. Bird, B. and J. Rowlette, *A protocol for rapid, label-free histochemical imaging of fibrotic liver*. Analyst, 2017. **142**(8): p. 1179-1184.
112. Varma, V.K., et al., *A label-free approach by infrared spectroscopic imaging for interrogating the biochemistry of diabetic nephropathy progression*. Kidney Int, 2016. **89**(5): p. 1153-1159.

113. Krishnakumar, N., et al., *Screening of chemopreventive effect of naringenin-loaded nanoparticles in DMBA-induced hamster buccal pouch carcinogenesis by FT-IR spectroscopy*. Mol Cell Biochem, 2013. **382**(1-2): p. 27-36.
114. Janik, M.E., A. Litynska, and P. Vereecken, *Cell migration-the role of integrin glycosylation*. Biochim Biophys Acta, 2010. **1800**(6): p. 545-55.
115. Nakerakanti, S. and M. Trojanowska, *The Role of TGF-beta Receptors in Fibrosis*. Open Rheumatol J, 2012. **6**: p. 156-62.
116. Lazenby, A.J., et al., *Remodeling of the lung in bleomycin-induced pulmonary fibrosis in the rat. An immunohistochemical study of laminin, type IV collagen, and fibronectin*. Am Rev Respir Dis, 1990. **142**(1): p. 206-14.

Office of Animal Care and Institutional
Biosafety Committee (OACIB) (M/C 672)
Office of the Vice Chancellor for Research
206 Administrative Office Building
1737 West Polk Street
Chicago, Illinois 60612

12/15/2016

Viswanathan Natarajan
Pharmacology
M/C 868

Dear Dr. Natarajan:

The protocol indicated below was reviewed in accordance with the Animal Care Policies and Procedures of the University of Illinois at Chicago and renewed on 12/15/2016.

Title of Application: Mechanisms of Acute Lung Injury
ACC NO: 15-240
Original Protocol Approval: 1/15/2016 (3 year approval with annual continuation required).
Current Approval Period: 12/15/2016 to 12/15/2017

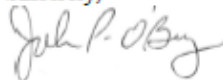
Funding: Portions of this protocol are supported by the funding sources indicated in the table below.
Number of funding sources: 2

Funding Agency	Funding Title			Portion of Funding Matched
NIH	Role of sphingolipids in the pathobiology of lung injury (Project 1)			Protocol is linked to form G 16-184
Funding Number	Current Status	UIC PAF NO.	Performance Site	Funding PI
P01 HL098050	Funded	2010-07207	UIC	Viswanathan Natarajan
Funding Agency	Funding Title			Portion of Funding Matched
NIH	Restoration of lung vascular barrier integrity			Protocol is linked to form G 16-059
Funding Number	Current Status	UIC PAF NO.	Performance Site	Funding PI
P01 HL060678 (yrs 16-20 AI version)	Funded	2016-02251	UIC	Asrar Malik/Viswanathan Natarajan (Project 4)

This institution has Animal Welfare Assurance Number A3460.01 on file with the Office of Laboratory Animal Welfare, NIH. This letter may only be provided as proof of IACUC approval for those specific funding sources listed above in which all portions of the grant are matched to this ACC protocol.

Thank you for complying with the Animal Care Policies and Procedures of the UIC.

Sincerely,



John P. O'Bryan, PhD
Chair, Animal Care Committee
JPO/kg

cc: BRL, ACC File, Panfeng Fu, Longshuang Huang, Anantha Harijith

Begin forwarded message:

From: Jürgen Popp <em@editorialmanager.com>
Subject: Decision on your submission to Journal of Biophotonics (jbio.201700383)
Date: January 27, 2018 at 8:31:13 AM CST
To: Michael Walsh <galahm@uk.edu>
Reply-To: Jürgen Popp <jpo@uni-jena.de>

Dear Dr. Walsh,

Thank you for submitting your manuscript "Fourier transform infrared imaging to identifies biochemical changes in pulmonary fibrosis in a label-free manner" to Journal of Biophotonics. The reviewer report and comments are included at the end of this email.

On the basis of the reviewer comments, we are not able to accept your manuscript for publication at this stage. However, we believe that your manuscript might become acceptable for publication after major **revisions**, if you are able to address the reviewer comments and make the necessary **revisions** and improvements.

To submit your **revision**, go to <https://jbio-journal.editorialmanager.com/> and log in as an Author using your username (MichaelWalsh) and password. Your submission can be found under the menu item "Submissions Needing Revision".

Please note that when you submit the **revised** version of this manuscript, you will be asked to upload a zip archive containing the production data that will be used if your manuscript is accepted. See below for more details. When you submit your **revised** manuscript, please include a point-by-point response to the reviewer comments in the "Respond to Reviewers" box, including a list of changes made and a rebuttal to any comments with which you disagree. All changes to your manuscript should also be highlighted in the main manuscript file.

We should receive your **revised** manuscript by 26 Feb 2018. Please inform us if you anticipate you will need more time.

We look forward to receiving your **revised** manuscript.

Yours sincerely,

Jürgen Popp

P.S. To avoid delays in the processing of your manuscript please provide a pdf as well as the source files (Word and separate image files or the respective LaTeX EPS package). For preparation guidelines see [http://onlinelibrary.wiley.com/journal/10.1002/\(ISSN\)1964-0649/homepage/2475_Author_Guidelines.html](http://onlinelibrary.wiley.com/journal/10.1002/(ISSN)1964-0649/homepage/2475_Author_Guidelines.html)

If your manuscript includes Supporting Information, please upload this as a separate file.

If you have not yet done so, please also upload an eye-catching color image for the graphical abstract (ideal size: 5cm x 5cm). It can be one from your manuscript or specifically designed for the purpose, but should not show too many details or consist of several parts. Also enclose a short descriptive and popular text on the general aim and value of your paper which may serve as an 'appetizer' for the readers (up to 70 words, not a figure caption, not the abstract text). It should be written in impersonal or passive style. For Review Articles and Full Papers: enclose a short CV and a photo of each author as Supporting Information.

REVIEWER REPORT:

Please note that reviewers may not be numbered consecutively.

COMMENTS TO AUTHOR:

Reviewer #1: A timely and interesting study - there are a number of points I feel need attention in a **revised** manuscript.
Abstract FTIR abbreviation should follow right after its meaning
Were the ratios calculated after the second-order differentiation? Spectral ratios should be calculated before this step to avoid over-processing and 'distortion' of the data.
Is there a colour scale for Fig. 1K-1O?
The x-axis of Fig. 4C-4E are mislabelled and do not match the legend.

L-00320-2018 Receipt of New Paper by American Journal of Physiology-Lung Cellular and Molecular Physiology 

 alplung@msubmit.net
to me (2)

Jul 16 (8 days ago)   

Dear Dr. Suryadevara,

On 16th Jul 2018, I received your manuscript entitled "Phospholipase D Regulates Bleomycin-Induced Pulmonary Fibrosis via Alveolar Epithelial Cell Mitochondrial ROS and DNA Damage" by Vidyani Suryadevara, Longshuang Huang, Seock-Jo Kim, Paul Cheresch, Mark Shaaya, Mounica Bandela, Panfeng Fu, Carol Feighal-Bostwick, Gilbert Di Paolo, David Kamp, and Viswanathan Natarajan.

Your manuscript has been assigned the Paper #: L-00320-2018.

You may check on the status of this manuscript by selecting the "Check Manuscript Status" link under the following URL:

<https://ajplung.msubmit.net/cgi-bin/main.clix?ei=A1Dm2qM3ASDQoY7E7A9htd383JmYBWTZSZSLbqkOZ>

(Press/Click on the above link to be automatically sent to the web page.)

Thank you for submitting your work to the American Journal of Physiology-Lung Cellular and Molecular Physiology.

Sincerely,

Confidentiality Notice: This e-mail message, including any attachments, is for the sole use of the intended recipient(s) and may contain confidential and privileged information. Any unauthorized review, copy, use, disclosure, or distribution is prohibited. If you are not the intended recipient, please contact the sender by reply e-mail and destroy all copies of the original message.

Vidyani Suryadevara, PhD

Education:

University of Illinois, Chicago Bioengineering	PhD	2018
University of Illinois, Chicago Bioengineering	M.S.	2014
Osmania University, Hyderabad, India Biotechnology	B.Tech	2013

Current and previous appointments:

Research Scientist, 05/18 – present

Department of Pharmacology, College of Medicine, University of Illinois, Chicago

Research Assistant, 01/16 – 05/18

Department of Bioengineering and Pharmacology, College of Medicine, University of Illinois, Chicago

Teaching Assistant, 01/14 – 01/16

Department of Microbiology, College of Liberal Arts & Sciences, University of Illinois, Chicago

Fellowships and Awards:

1. Chancellor's graduate research award 01/17 - 07/17 \$5000
2. Center for clinical and translational science Pre-doctoral education for clinical and translational scientists fellowship. 08/16 – 07/17 \$ 32,100
3. Provost Deiss Award for Biomedical Research 04/15 \$3000
4. President's Volunteer Service Award 06/18
5. Competent Communicator, Toastmasters International 05/18
6. Competent Leader, Toastmasters International 05/18
7. ASBMB travel award for Experimental Biology Conference 2018 04/18
8. Eugertha Bates Memorial Award, UIC 04/18
9. Best Teacher Award, Women Empowerment Campaign Chicago 03/18
10. Honorable Mention Certificate Winner in the Graduate, MD/PhD and other combined degree category at the COM Research Forum 2015. 12/15
11. Graduate Student Council Travel Award, Graduate College Student Presenter Award 2015-2018
12. Chancellor's Award for Student Service & Leadership, Student leadership award, UIC 2014-2018

Publications:

Submitted:

1. **Suryadevara V**, Huang LS, Kim SJ, Cheresh P, Shaaya M, Bandela M, Fu P, Feghali BC, Paolo DG, Kamp DW, Natarajan V Phospholipase D Regulates Bleomycin-Induced Pulmonary Fibrosis via Alveolar Epithelial Cell Mitochondrial ROS and DNA Damage (FASEB)
2. Ebenezer DL, Berdyshev E, Bronova IA, Liu Y, Tiruppathi C, Komorova Y, Benevolenskaya E, **Suryadevara V**, Ha AW, Harijith A, Tudor R, Huang Y, Naren A, Natarajan V, Fu P Pseudomonas aeruginosa stimulates nuclear S1P generation and epigenetic regulation of lung inflammation

(Thorax).

3. **Suryadevara V**, Nazeer SS, Sreedhar H, Natarajan V, Walsh MJ Fourier transform infrared imaging identifies biochemical changes in pulmonary fibrosis in a label-free manner (American Journal of Pathology)

Published:

1. Fu P, Ebenezer DL, Ha AW, **Suryadevara V**, Harijith A, Natarajan V. 2018. Nuclear lipid mediators: Role of nuclear sphingolipids and sphingosine-1-phosphate signaling in epigenetic regulation of inflammation and gene expression. J Cell Biochem.
2. **Suryadevara V**, Fu P, Ebenezer DL, Berdyshev E, Bronova IA, Huang LS, Harijith A, Natarajan V. 2018. Sphingolipids in Ventilator Induced Lung Injury: Role of Sphingosine-1-Phosphate Lyase. Int J Mol Sci 19.
3. Ebenezer DL, Fu P, **Suryadevara V**, Zhao Y, Natarajan V. 2017. Epigenetic regulation of pro-inflammatory cytokine secretion by sphingosine 1-phosphate (S1P) in acute lung injury: Role of S1P lyase. Adv Biol Regul 63: 156-166.
4. Testai FD, Xu HL, Kilkus J, **Suryadevara V**, Gorshkova I, Berdyshev E, Pelligrino DA, Dawson G. 2015. Changes in the metabolism of sphingolipids after subarachnoid hemorrhage. J Neurosci Res 93: 796-805.
5. **Suryadevara V**, Govindkumari V 2015 Exosomes and microparticles: the nanosized vesicles released from the cells that act as biomarkers for disease and treatment – riveting on lung diseases Mater. Today Proc., 2: 4626-4631

Book: Vidyani Suryadevara, Sreenivas Reddy Beemi Nanotechnology: Principles and Applications ISBN: 978-93-85100-58-1 Paramount Publishing House 2017

Professional Associations:

1. American Society for Biochemistry and Molecular Biology
2. American Heart Association *Scientific Council Affiliation(s)*: Council on Cardiopulmonary, Critical Care, Perioperative and Resuscitation
3. American Thoracic Society.
4. American Association for the Advancement of Science.
5. Society for Women in Engineering
6. Women in Science and Engineering.

University service:

1. President, Graduate student council, UIC 2016-18
 - Member, Student fee advisory committee 2013-18
 - Search advisory Committee, Vice-Chancellor for Health Affairs 2015
 - Search advisory Committee, Vice-Chancellor for research 2017
 - Higher Learning Commission Assurance Argument Committee
 - UIC budget advisory committee
2. President, College of Engineering Toastmasters club 2015-18

- | | |
|--|-----------|
| 3. Treasurer, Graduate Student Council, UIC | 2014-2016 |
| ▪ Managed the annual budget of GSC | |
| ▪ Approved and processed travel awards and projects awards | |
| 4. President, Indian Society for Technical Education, CBIT Chapter | 2011-2013 |
| 5. President, Chaitanya Bharathi Cultural Club | 2010-2013 |

Conference Presentations:

- Stainless imaging to identify the biochemical changes during bleomycin-induced pulmonary fibrosis by Fourier transform infrared technique at Experimental Biology 2018 conference, **San Diego, CA**
- Poster presentation on stainless computed histopathology of bleomycin-induced pulmonary fibrosis by Fourier transform infrared technique at pulmonary fibrosis foundation summit 2017 at **Nashville, TN**
- Scientific Interest Group Poster Discussion and Networking Session on Phospholipase D Regulates GSK3 β Mediated Epithelial to Mesenchymal Transition and Akt Mediated Cell Death Leading to Pulmonary Fibrosis at Experimental Biology 2017 Conference, **Chicago, IL**
- Poster presentation on ‘Elucidating the opposing regulatory role of phospholipase D in alveolar apoptosis and myofibroblast differentiation in pulmonary fibrosis’ in the International Colloquium on lung and airway fibrosis (ICLAF 2016) in **Dublin, Ireland** from 23rd -28th September 2016.
- **Thematic** poster in the session ‘Lung fibrosis: new directions to inform the future’ at 2016 ATS international conference in San Francisco, CA from 13-18th May 2016.
- Poster presentation on ‘Role of phospholipase d in idiopathic pulmonary fibrosis’ at the Combined Annual Meeting of CSCTR and MWAFFMR, April 21-22, 2016, at the Mid-America Club in Chicago, IL.
- Oral presentation in ‘VILI and regional lung effects of mechanical ventilation’ session at 2015 ATS International Conference in **Denver, Colorado** from 15-18 May 2015.
- Invited talk on ‘Therapeutic intervention of sphingolipids in ventilator-induced lung injury’ in International Conference on Recent Advances in Research and Treatment of Human Diseases at Hyderabad, India from 9th -11th January 2015.
- Anantha Harijith, Xiaoguang Sun, Yangbasai Dong, David Ebenezer, Vidyani Suryadevara, Panfeng Fu, Longshuang Huang, Sekhar Reddy, J. Usha Raj, Joe G.N. Garcia, Viswanathan Natarajan. S1P Receptor1 Mediates Hyperoxia Induced Lung Injury in Newborn Mouse Model Pediatric Academic Societies (PAS) Annual Meeting April 28, 2015

Mentees:

Mentored and trained a masters’s student, several undergraduate, high school students in research.

1. Mounica Bandela, M.S. in Bioengineering (2017-2018).
2. Kavya C. Yarlagadda, PharmD student (Summer 2017)
3. Viraja Alluri, High School Student, (Summer 2016, 2017).
4. Hajra Ashur A.Takala, MPH, M.B.B.Ch (Summer 2016)

5. Jan Mangulabnan, Illinois Math and Science Academy (Summer 2016).
6. James Da Silva Pinheiro, visiting undergraduate student from Brazil (Summer 2015).
7. Azadeh Taghizadeh Khamesi, undergraduate student, UIC (Summer 2015).
8. Meghana Machireddy, High School Student (Summer 2014) *Current Position*: BS Student, Cornell University.

Techniques:

Molecular biology: Western blot, PCR, qRT-PCR, Genotyping, siRNA mediated silencing of genes; *Immunology*: Cytokine analysis by ELISA, immunofluorescence, immunoprecipitation; Handling of human clinical samples: Microparticles isolation; Cell culture, Nucleus isolation; *Magnetic resonance imaging*; *Fourier Transform Infrared Imaging and data preprocessing and analysis*; *Animal models*: Isolation of fibroblasts from mice; Maintenance and breeding of colonies, generation of flox mice as well as whole body knock-out mice, Instillation of bleomycin intratracheally to develop bleomycin induced pulmonary fibrosis model, Ventilator induced lung injury murine model, animal surgeries, lung harvesting and BALF collection; *Microbiology*: aseptic handling, identification of evaluation of unknown microorganisms including bacteria, fungi, actinomycetes.